ACS OMEGA

Open Access

http://pubs.acs.org/journal/acsodf

Article

Biosynthesis of *Artemisia abyssinica* Leaf Extract-Mediated Bimetallic ZnO−CuO Nanoparticles: Antioxidant, Anticancer, and Molecular Docking Studies

Temesgen Achamo Orshiso,* Enyew Amare Zereffa,* H. C. Ananda Murthy,* Taye B. Demissie,* Onkar Pardeshi, Lata S. Avhad, and Suresh Ghotekar

Cite This: *ACS Omega* 2023, 8, 41039−41053

Read Online

ACCESS | Metrics & More | Article Recommendations

ABSTRACT: Currently, plant extract-mediated synthesized metal oxide nanoparticles (MO NPs) have played a substantial role in biological applications. Hence, this study focused on the eco-benign one-pot synthesis of bimetallic ZnO−CuO nanoparticles (ZC NPs) using the leaf extract of *Artemisia abyssinica* (LEAA) and evaluations of their anticancer, antioxidant, and molecular binding efficacy. The optical absorption peak at 380 nm from UV−visible (UV−vis) analysis revealed the formation of ZC NPs. X-ray diffraction (XRD) results revealed the fabrication of mixed-phase crystals with hexagonal and monoclinic structures of ZC NPs with an average crystallite size of 14 nm. Moreover, the biosynthesis of ZC NPs with a spherical morphology and an average particle size of 13.09 nm was confirmed by scanning electron microscopy (SEM), energy-dispersive X-ray (EDX), and transmission electron microscopy (TEM) results. Fourier transform infrared (FTIR) and thermogravimetric analysis (TGA/DTA) spectroscopy confirmed the involvement of functional groups from LEAA during the synthesis of ZC NPs. ZC NPs have exhibited the ferric ion reducing power (FRAP) with an absorbance of 1.826 ± 0.00 at 200 μg/mL and DPPH (2,2-diphenyl-1-picryl-hydrazyl-hydrate) radical scavenging activity of 95.71 ± 0.02% at 200 μg/mL with an IC50 value of 3.28 μg/mL. Moreover, ZC NPs had shown a promising in vitro anticancer activity of 89.20 ± 0.038 at 500 μg/mL with an IC50 value of 33.12 μg/mL against breast cancer (MCF-7) cell lines. Likewise, ZC NPs have shown strong binding affinity (−8.50 kcal/mol) against estrogen receptor α (ERα) in molecular docking simulations. These findings suggested that the biosynthesized ZC NPs could be used as promising antioxidant and anticancer drug candidates, particularly for breast cancer ailments. However, the *in vivo* cytotoxicity test will be recommended to ensure further use of ZC NPs.

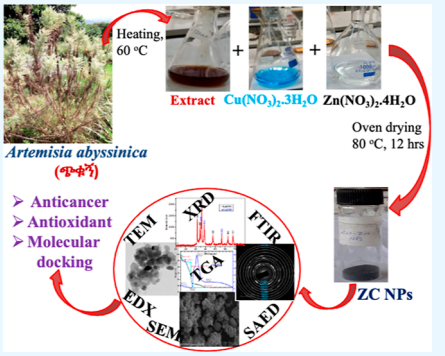

1. INTRODUCTION

Cancer and oxidative stress-induced ailments have been among the main causes of global morbidity and deaths for a very long time.[1] Cancer is often a deadly disease that burdens society tremendously, in both developing and developed countries.[2] Oxidative strain is typically prompted by the presence of disproportionate reactive oxide species (ROS) and affects body cell functions in a number of ways.[3,4] Oxidative strain can eventually lead to the progress of multifarious pathological problems, including cancer, diabetes, acute renal failure, arthritis, neurodegenerative diseases, respiratory system impairment, cardiovascular problems, aging, and inflammatory disorders.[4] Numerous anticancer and antioxidant drugs have been introduced recently; however, the majority of them have encountered cytotoxicity to a healthy body, poor water solubility, restricted membrane transport, and limitations in rapid clearance in the bloodstream.[5] Due to ample challenges emanated, cancer and oxidative stress have become the main focus of the scientific community recently.[6]

Metal oxide nanoparticles (MO NPs) have been gaining the attention of researchers in the biological field due to their astonishing physicochemical properties such as high surface-to-volume ratio, enhanced surface charge, aqua solubility, colloidal stability, and biocompatibility.[7,8] Moreover, due to their significant catalytic, optical, electrical, and magnetic features and chemical stability, they have incredible intracellular tracking, stability in the biological milieu, and rapid clearance from biological fluids.[8,9] Likewise, the ability of MO NPs to produce a large number of reactive oxygen species (ROS) with great selectivity and lower sensitivity to normal cells is particularly important to curb the proliferation of

Received: March 17, 2023
Revised: September 10, 2023
Accepted: October 10, 2023
Published: October 24, 2023

cancerous cells.[10,11] Recently, the efficacy of numerous MO NPs in cancer and oxidative-stress-driven ailments has been broadly reported.[12,13]

However, due to their cost-effectiveness, structural activity, biocompatibility, and bioavailability, ZnO and CuO NPs have received special aspects among the various MO NPs in cancer and oxidative stress-induced ailments.[14,15] Owing to their surface crystal defects and semiconductive nature of these nanoparticles, the electrons move easily and could react with oxygen species to form free radicals, which in turn cause oxidative stress in cancerous cells.[16,17] Because of their inherent electrostatic nature and selective toxicity, ZnO NPs are more apposite in cancer therapy.[18] ZnO nanoparticles have exhibited significant anticancer efficacies against a variety of cancer types, including lung cancer,[19] breast cancer,[20] ovarian cancer,[21] and colorectal cancer.[22] The anticancer potency of ZnO NPs is mainly through zinc-mediated protein activity disequilibrium and oxidative stress.[23] Recently, it has been reported that the enhanced anticancer efficacy of CuO NPs is against breast cancer,[24] hepatocellular carcinoma,[25] lung cancer,[26] and cervical cancer.[27] The anticancer mechanism of CuO NPs is mainly through genotoxicity and apoptotic death in cancerous cells due to their ability to generate enhanced ROS.[28] Moreover, the ZnO and CuO NPs have been also repeatedly reported as significant antioxidant agents.[15,29,30] However, due to their enhanced synergistic effects, including enriched surface area, multiple reactive sites, higher charge flow, and mass transfer, the integration of ZnO and CuO NPs together is preferred over their monometallic counterparts.[16,31,32]

Nevertheless, the methods of synthesis of MO NPs are the noticeable factors that determine their efficiency in biological use. Various methods, such as physical, chemical, and biological approaches, have been utilized for the fabrication of MO NPs.[12,33] However, physical and chemical approaches have noticeable limitations, including high energy consumption, utilization of toxic solvents, small yield production, extra time, and increased cost demand. Due to the stated constraints of conventional methods, the researchers paved the way for a new approach with less energy, time, and cost demands. The biological (green) synthesis approach is cost-effective, facile, and eco-benign and also prohibits the immersion of toxic chemicals into living entities.[15,30] The biosynthesis of MO NPs has been employed using diverse biosystems, such as plant extracts, bacteria, fungi, and large biological molecules. However, using plant extracts has a low handling cost, safer, and is an easy technique to fabricate NPs on a large scale in comparison with bacterial and fungal strains.[34,35] Furthermore, the multifarious functional groups from phytochemicals of plant extracts, counting NH_2, SH, COOH, C═O, and OH, are used as greener and stronger reducing and capping agents.[36,37] Using medicinal plants for the synthesis of NPs can also exhibit further synergistic effects on biological activity.[12,38]

This work focuses on the fabrication of facile, eco-benign, and one-pot biosynthesis of bimetallic ZnO−CuO (ZC) NPs using a greener reducing and capping agent from the LEAA and the evaluation of its biological efficacy. *Artemisia abyssinica* belongs to the family *Asteraceae* and is an indigenous plant used in folk medicine for the treatment of various ailments such as inflammation, cold, gonorrhea, headache, stomachache, anorexia, fever, and dysmenorrhea in Ethiopia.[39] Moreover, the plant has also been reported as an antimalarial, antiparasitic, antitumor, antirheumatic, anti-inflammation, and antioxidant agent.[40] The main contents of phytochemicals investigated in the leaf part of *A. abyssinica* are polyphenols, alkaloids, flavonoids, tannins, terpenoids, saponins, and essential oils.[36,41]

Hence, in this study, we reported *A. abyssinica* leaf extract-mediated synthesis and characterization of ZC NPs using advanced techniques like UV−vis, FTIR, TGA, XRD, SEM, EDX, and TEM. The as-synthesized ZC NPs have been investigated for their antioxidant potentials through FRAP and DPPH assays and their anticancer efficacy against MCF-7 cell lines in the MTT assay. Further, molecular docking studies of biosynthesized ZC NPs have been evaluated against estrogen receptor alpha (ERα; PDB: 5GS4) using the AutoDock 4.2 (MGL tools 1.5.7) program.

2. MATERIALS AND METHODS

2.1. Chemicals and Media. The chemicals zinc nitrate [$Zn(NO_3)_2{\cdot}4H_2O$, 99.9%], copper nitrate [$Cu(NO_3)_2{\cdot}3H_2O$, 99.8%], ethanol (C_2H_6O, 99.9%), sodium hydroxide (NaOH, 97%), 2,2-diphenyl-1-picryl-hydrazyl-hydrate (DPPH), and ascorbic acid, Sigma-Aldrich, were purchased from Addis Ababa, Ethiopia. Breast cancer (MCF-7) cells, peripheral blood mononuclear cells (PBMCs), Dulbecco's modified Eagle medium (DMEM), fetal bovine serum (FBS), and 3-(4,5-dimethylthiazol-2-yl)-2,5-diphenyltetrazolium bromide (MTT) PenStrep, Trypsin, Spectramax I3X, CO_2 incubator, and Doxorubicin (Invitrogen, USA) were obtained from India.

2.2. Preparation of Plant Extract. The preparation of plant extract was done according to our previous work with certain modifications.[36] The leaves part of the medicinal plant *A. abyssinica* was collected from Tiyo Woreda, Arsi Zone, on September 2022. Tiyo Woreda, demarcated (7°45′55″ and 8°02′02″N latitude and 38°56′42″ to 39°18′31″E longitude), is found in Arsi Zone, Oromia Region, Ethiopia, which is located at 175 km southeast of Addis Ababa with an elevation range of 1850 to 4050 m.[35] The collected plant was authenticated by a botanist and deposited in the National Herbarium, Addis Ababa University, with voucher specimen number YC008. The leaves of *A. abyssinica* were washed with tap and distilled water repeatedly and dried for 13 days in the dark to remove the moisture content. After grinding with a mechanical grinder, 10 g of powdered leaves was mixed with 100 mL of 50% ethanol (water and ethanol, 1:1 v/v) in 250 mL conical flasks. The mixtures were shaken for 1.5 h at 120 rpm and 25 °C in a mechanical shaker and then heated for 50 min at 60 °C with a magnetic stirrer. After centrifuging the obtained crude extract to produce a clear solution, the mixture was cooled at room temperature for an overnight period before being filtered through Whatman filter paper. A clear brown color extract was eventually obtained and preserved at 4 °C for further study.

2.3. One-Pot Green Preparation of ZC NPs. 0.1 M mixed salts [$Cu(NO_3)_2{\cdot}3H_2O$ and $Zn(NO_3)_2{\cdot}4H_2O$] solution was mixed with prepared LEAA in a proportion of 3:1 (v/v) by stirring vigorously. According to optimizations of our previous study,[36] the solution was adjusted at pH 5 and heated for 1 h at 70 °C on a hot plate containing a magnetic stirrer. The light blue to reddish brown color change has been observed for the spontaneous reduction and formation of ZC NPs. Following the reaction, the mixture was sonicated at room temperature for 1 h at 60 rpm in order to keep the dispersion of particles. After sonication, the reaction mixture was centrifuged for 20 min at 6000 rpm. The obtained pellets were washed repeatedly with distilled water, following ethanol in order to remove the

https://doi.org/10.1021/acsomega.3c01814
ACS Omega 2023, 8, 41039−41053

impurities, and then oven-dried at 80 °C for 12 h. Finally, the black-brown powder was obtained and stored in proper containers at 4 °C for further analysis.[42]

2.4. Characterizations. An ultraviolet−visible (UV−vis, SM-1600) spectrophotometer in the wavelength region 200−800 nm was used to identify the SPR (surface-plasmon resonance) spectra of as-synthesized ZC NPs. A BRUKER D8 Advance XRD, AXS GMBH, and Karisruhe, West Germany, equipped with a Cu target for generating a Cu Kα radiation (wavelength 1.5406 Å) at GSE was used to analyze the size and crystalline nature of biosynthesized ZC NPs. Using Fourier transform infrared (FTIR Shimadzu, Japan 8400S) spectroscopy with the potassium bromide (KBr) disk in the 400 and 4000 cm^{-1} wavenumber region; the potential phytochemicals responsible for the reductions and stabilizations of metal salts into ZC NPs were examined. Moreover, the weight loss and existing biomolecules of biosynthesized ZC NPs were analyzed by a thermogravimetric analyzer TGA/DTA (DTG 60H Shimadzu, Japan), by heating at 35−800 °C. The surface features, morphology, and elemental compositions of ZC NPs were analyzed by using scanning electron microscopy combined with energy-dispersive X-ray spectroscopy (SEM−EDX, Tescan Mira 3 LMU). Transmission electron microscopies in combination with selected area electron diffraction (TEM/HRTEM-SAED, JEOL, JEM-210, 200 kV, LaB6 filament, and EDS-1.5 Å TEM resolution) were also used to characterize the particle size and internal morphology of as-synthesized ZC NPs.

2.5. Biological Activity of ZC NPs. *2.5.1. Antioxidant Activity Test.* Ferric reducing antioxidant power (FRAP) and 1,1-diphenyl-2 picrylhydrazyl (DPPH) assays were used to evaluate the antioxidative properties of precursor salts (copper nitrate, zinc nitrate), and ZC NPs.

2.5.1.1. Ferric Reducing Antioxidant Power Assay. By using the ferric reducing antioxidant power (FRAP) assay, the *in vitro* antioxidant activity of precursor salts and ZC NPs was evaluated.[43,44] Different concentrations (200, 100, 50, 25, and 12.5 μg/mL, in H_2O) of each sample were mixed with 0.2 M potassium phosphate buffer (2 mL, pH 6.6) and potassium ferricyanide (2.5 mL, 10% w/v) solutions, followed by incubation at 40 °C for 30 min. After centrifuging the incubated solutions for 10 min at 3000 rpm with trichloroacetic acid (2.5 mL, 10% w/v) added, a supernatant (5 mL) of each solution was combined with distilled water (2 mL) and ferric chloride (0.5 mL, 0.1% w/v). Using a UV−visible spectrophotometer, the absorbance of each solution was measured at 700 nm. The measurement of absorbance was carried out in triplicate and used to calculate the ferric ion reducing power mean ± standard deviation of each sample.

2.5.1.2. DPPH Assay. The *in vitro* antioxidant activity of precursor salts and ZC NPs was also evaluated using a DPPH assay.[36,45] The DPPH stock solution was prepared by dissolving 4 mg of DPPH in 100 mL of methanol and stored at 4 °C in the dark condition for 3 h to test the stability of the solution. Constant λ max of the solution observed at 517 nm revealed that the solution was stable throughout the experiment. Two mL of 0.1 mM DPPH solution was mixed with 1 mL (200, 100, 50, 25, and 12.5 μg/mL) of $Zn(NO_3)_2{\cdot}4H_2O$, $CuNO_3{\cdot}3H_2O$, extract, ZC NPs, and ascorbic acid solutions. The reaction solutions were mixed and incubated for 30 min at 27 ± 2 °C in the dark. Ascorbic acid and methanol were used as positive control and a blank, respectively. By using a UV−visible spectrophotometer, the absorbance of each solution was recorded at 517 nm. Also, each measurement was conducted in triplicate, and the results were expressed as the mean ± standard deviation.

Equation 1 was used to compute the DPPH radical scavenging abilities of the precursor salts, ZC NPs, and ascorbic acid.

$$\text{DPPH scavenging activity (\%)} = \frac{\text{AB} - \text{AS}}{\text{AB}} \times 100 \quad (1)$$

where AB is the absorbance of the blank and AS is the absorbance of the sample.

2.5.2. Anticancer Activity Test. 2.5.2.1. Culturing of Cells. The breast cancer (MCF-7) and peripheral blood mononuclear (PBM) cells were obtained from the National Center for Cell Sciences (NCCS), India. By using the standard method, MCF-7 and PBM cells were cultured.[46] The standard cells were hatched in DMEM at 37 °C in 5% CO_2 and injected with 10% (v/v) fetal bovine serum (FBS), penicillin (100 IU/mL), and streptomycin (100 g/mL) until they become confluence. The cell was separated with a cell dissociating solution (0.2% trypsin, 0.02% EDTA, 0.05% glucose in PBS). After testing the viability of the cells, they were centrifuged. Furthermore, 5×10^4 cells/well were cultivated in a 96-well plate and nurtured for 24 h at 37 °C under a 5% CO_2 incubator.

2.5.2.2. Cytotoxicity Test. The 3-(4,5-dimethylthiazol-2-yl)-2, 5-diphenyltetrazolium bromide (MTT) test was used to determine the *in vitro* cytotoxicity of ZC NPs and doxorubicin on PBM and MCF-7 cells.[47] The standard cells were trypsinized and adjusted with 5×10^4 cells/ml to count cells by using respective media containing 10% FBS (v/v). The diluted cell suspension (5×10^4 cells/well) was added to each of the 96 wells of the microliter plate in a quantity of 100 μL. After incubation, the test solutions in the wells were rejected, and 0.05 mg of MTT was added to each well. The plates were kept for 4 h at 37 °C under a 5% CO_2 atmosphere.

The resulting formazan was dissolved in 100 μL of dimethyl sulfoxide (DMSO) with gentle shaking at 37 °C. The absorbance was measured using a microplate reader at 570 nm. Equation 2 was used to compute the percentage growth inhibition, and the dose−response curves for each cell line were used to obtain the IC50 values. Each experiment was carried out in triplicate, and the resulting cell growth inhibitions were analyzed as the mean ± standard deviation.

$$\text{\% inhibition} = ((\text{OD of control} - \text{OD of sample}) / \text{OD of control}) \times 100 \quad (2)$$

2.5.3. Molecular Docking. Molecular docking studies of biosynthesized ZC NPs and the standard drug (doxorubicin) were evaluated against estrogen receptor alpha (ERα; PDB: 5GS4) by the AutoDock 4.2 (MGL tools 1.5.7) program.[48,49] The crystal structures of estrogen receptor alpha (ERα; PDB: 5GS4) of breast cancer were downloaded from the protein database and processed by removing the cocrystallized ligand, deleting water molecules, and adding polar hydrogen and cofactors according to the AutoDock 4.2 (MGL tools 1.5.7) technique. After the protein was cleaned, only polar hydrogens and the Kollman charges were introduced. In line with the experiment, we used doxorubicin as a control standard drug. The grid center coordinates were 65, 65, and 65 pointing in the x, y, and *z* directions, respectively, with a grid point spacing of 0.375 Å. The center grid boxes were −12.055, −10.491, and

https://doi.org/10.1021/acsomega.3c01814
ACS Omega 2023, 8, 41039−41053

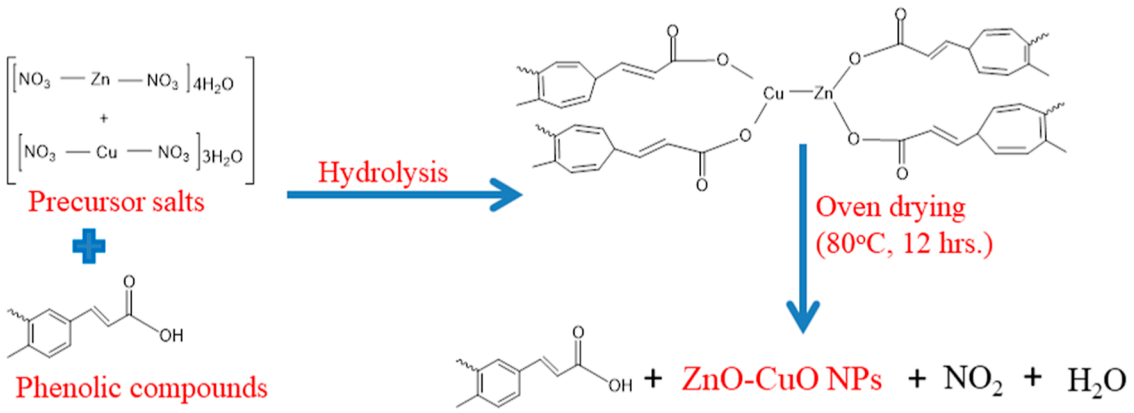

Figure 1. Schemes of the reaction mechanism of ZC NP formation.

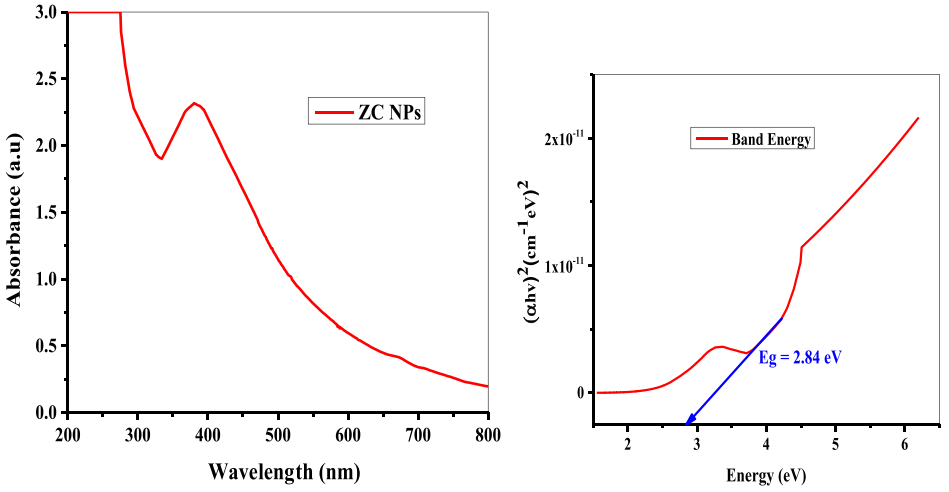

Figure 2. UV−visible optical absorption spectra of ZC NPs (left) and Tauc plot (right).

5.964 Å. The synthesized molecules were built as a pdb file using Gaussian software. Gasteiger charges and Kollman united atom charges were added to the ligands and receptors, respectively. 100 different conformations were generated for the targeted ZC NPs and the standard drug. The conformation of the ZC NPs and standard drug with the lowest free binding energy was selected to analyze their interactions with the receptors by using the Discovery Studio Visualizer.

2.6. Statistical Data Analysis. All the experimental results were computed using the one-way analysis of variance (ANOVA) function of the statistical package for social science (SPSS) version 20 and presented as the mean ± standard deviation for triplicate experiments. The docking studies of nanoparticles and the target were evaluated by the AutoDock 4.2 (MGL tools 1.5.7) program. Data analysis was also done with ImageJ (imajej153-win java8 imagej.exe), Gatan Microscopy Suite software (GMS 64 bit) version 2.x, and Origin software (Originpro 9.0 64 bit).

3. RESULTS AND DISCUSSION

3.1. Biosynthesis of ZC NPs. Biosynthesis of ZC NPs was performed by using ethanolic (50%, v/v) LEAA as a reducing and stabilizing agent. The change in color from blue [$Cu(NO_3)_2{\cdot}3H_2O$], colorless [$Zn(NO_3)_2{\cdot}3H_2O$], and dark brown (pure extract) to black-brown was observed and which visually exhibited the synthesis of ZC NPs. Aside from the color change, a distinctive optical absorption band at 380 nm presented in Figure 2 (right) corroborates the formation of ZC NPs via the green route.[50−52]

The proposed reaction mechanism of the biosynthesis of ZC NPs from precursor salts and LEAA is presented in Figure 1. The major phytochemicals present in LEAA are phenolic compounds such as polyphenols, alkaloids, flavonoids, and tannins, which are used as ligand agents.[36] Among the major active compounds, as also confirmed in the discussion parts from FTIR of this study, polyphenols are the possible agents that participate as reducing and capping ligands. However, polyphenols most commonly contain phenolic acids, stilbenes, and lignin groups. Among the phenolic acids accounts for the majority of polyphenols in most reported literature and also are those with the most active sites than the rest.[53] Therefore, the scheme of the proposed reaction mechanism of formations of ZC NPs is presented as follows.

3.2. Characterizations of ZC NPs. *3.2.1. UV−Visible Spectrophotometry Analysis.* The surface plasma resonance (SPR) band of nanoparticles depends on their physicochemical properties, such as shape, size, and surface distribution, as well as the dielectric properties of the medium. UV−visible spectrophotometry spectra of ZC NPs Figure 2 (left), which displayed a strong SPR peak at the edge of 380 nm.[51,54] The SPR absorption may be due to the interaction of free electrons of the ZC NPs with the light wave. Recent studies reported that anisotropic particles show two or more SPR bands, while spherical nanoparticles show only a single SPR band,

https://doi.org/10.1021/acsomega.3c01814
ACS Omega 2023, 8, 41039−41053

depending on the shape of the NPs.[55] Hence, the single SPR peak in the UV−visible spectrum of ZC NPs illustrates the formation of iso-morphological particles.[56] Phytochemical constituents (phenolic compounds) from the LEAA are responsible for the bioreduction of precursor salts to ZC NPs.[36,57] The capping agents regulate the stability and functionalization of the ZC NPs in the medium in which they are suspended.[58] A similar pattern of SPR behavior in the range 350−400 nm was reported for ZnO and CuO nanoparticles by previous studies.[56,59]

The band gap of the ZC NPs was calculated from the Tauc plot Figure 2 (right) and is found to be 2.84 eV. The band gap energy of the biosynthesized ZC NPs has demonstrated a moderately amended value compared with early reported CuO and ZnO nanoparticles.[36,57] Several factors, such as the size-induced quantum confinement, charge carrier concentration, grain size, morphology, lattice strain, and orbital hybridization by combining different atoms from bimetallic nanoparticles, may contribute to the change in band gap value from their monometallic counterparts.[59]

3.2.2. XRD Analysis. The structural compositions and crystallographic nature of biosynthesized ZC NPs were examined by using an X-ray diffractometer (XRD), as depicted in Figure 3. The characteristic diffraction peaks with 2θ values

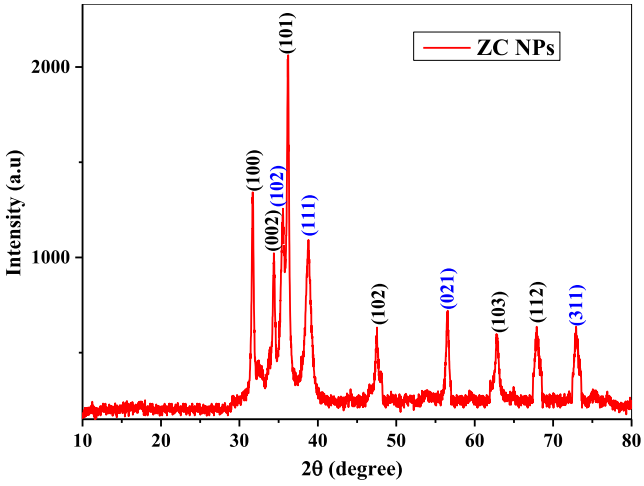

Figure 3. XRD pattern of biosynthesized ZC NPs.

of 31.71, 34.41, 35.56, 36.18, 38.79, 47.51, 56.50, 62.83, 67.89°, and 73.06 nm are associated with the Miller indices (hkl) values of (100), (002), (102), (101), (111), (102), (021), (103), (112), and (311), respectively. The typical diffraction peaks at (100), (002), (102), and (112) planes with 2θ values of 31.71, 34.41, 36.18, 47.51, 62.83, and 67.89° are associated with the crystalline structure of zinc oxide NPs with the (ICSD card no. 00-036-1451, Zincite-$P6_3mc$).[60] The diffraction peaks at (102), (111), (021), and (311) planes with peak positions of 35.56, 38.79, 61.82°, 56.50, and 73.06 nm are associated with the CuO NPs (ICSD card no. 00-048-1548, Tenorite-$C2/c$).[36,54] These XRD spectra are in alignment with early reported results and have revealed the successful synthesis of ZC NPs.[61] The sharper to broader diffraction peaks are observed, and the displayed (101), (100), (002), (002), (111), (200), (102), (110), (220), (311), and (222) planes are indicating the formation of the highly crystalline, hexagonal structure lattice with monoclinic symmetry of ZC NPs.[19] As seen in Figure 3, ZnO nanoparticles exhibit more distinct diffraction patterns and significant peak intensities in comparison to CuO NPs. This confirms that ZC NPs contain a greater portion of ZnO nanoparticles and a high degree of crystallinity, which is in line with the elemental composition observed in the EDX spectrum (Figure 7c).

The crystallite size (D) of the biosynthesized ZC NPs was calculated by using the Debye−Scherrer equation and Williamson−Hall plot as presented in Table 1. The average

Table 1. Crystallite Size (D) of ZC NPs and Microstrain (ε) from Debye−Scherrer and Williamson−Hall Calculations

Debye−Scherrer	Williamson−Hall plot	
average crystallite size (nm)	crystallite size (nm)	microstrain (ε) x 10^{-4}
13.85	14.94	8.32

crystallite size of ZC NPs calculated by the Debye−Scherrer eq (eq 3) was 13.85 nm.

$$D = \frac{K\lambda}{\beta \cdot \cos\ \theta} \tag{3}$$

where D, K, λ, β, and θ are the average crystallite size, the Scherrer constant (0.9), wavelength of X-ray (Cu Kα = 0.15418 nm), fwhm (full width at half-maximum), and Bragg's diffraction angle, respectively.

The crystallite size and microstrain of ZC NPs were also deconvoluted using the Williamson−Hall (W−H) model (eq 4).

$$\beta \cdot \mathrm{Cos}\ \theta = \frac{k.\ \lambda}{D} + 4\varepsilon\ \mathrm{Sin}\ \theta \tag{4}$$

where β is the full width of the Bragg peak at half-maximum (fwhm), θ is peak angle, D is mean crystallite size, k is the Scherrer constant, λ is the wavelength of X-ray, and ε is (microstrain). From this approach, the computed crystallite size and microstrain of ZC NPs are 14.94 nm and 8.32 × 10^{-4}, respectively. The obtained positive microstrain (slope) and extrapolating the linear fit to the y-intercept in Figure 4 indicate that the distances between the relevant crystal planes are not exactly the same, presumably as a result of the existence of tensile stress. The crystallite size of ZC NPs computed by the W−H approach is slightly greater than Scherrer's method.

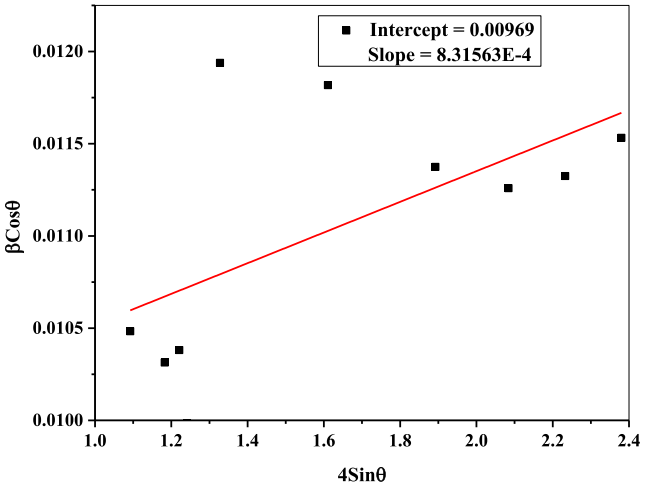

Figure 4. Linear fit of the ZC NPs Williamson−Hall plot.

https://doi.org/10.1021/acsomega.3c01814
ACS Omega 2023, 8, 41039−41053

This is because Scherrer's formula only predicts crystallite size based on averaging crystallite distribution from various peaks and does not consider the effects of peak expansion due to strain (ε).[62]

3.2.3. FTIR Analysis. Figure 5 presents the FT-IR spectra of LEAA, CuO, ZnO, and ZC NPs. All the as synthesized

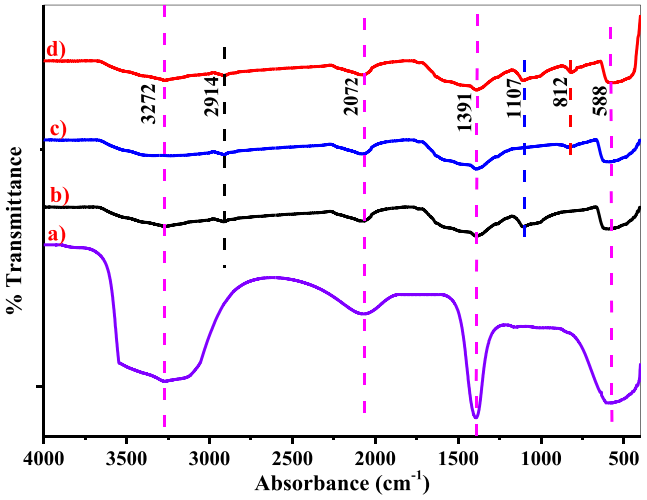

Figure 5. FTIR spectra of (a) LEAA, (b) CuO NPs, (c) ZnO NPs, and (d) ZC NPs.

nanoparticles, including the extract, have revealed similar absorption bands at 3272, 2072, 1391, and 588 cm^{-1}. The common small peak also appeared at 2914 cm^{-1} for the biosynthesized CuO, ZnO, and ZC NPs. Moreover, the common absorption bands at 1107 cm^{-1} with CuO and at 812 cm^{-1} with ZnO nanoparticles have appeared for the biosynthesized ZC NPs. The broad and intense peaks at 3272 and at 2914 cm^{-1} were attributed due to the vibrational stretching of O−H and of C═O from phenolic compounds of the LEAA, respectively.[36,63] The demanding peak at 2072 cm^{-1} is also ascribed due to the bending and stretching frequency of C≡C from terminal alkyl groups.[64] The intense peaks at 1391 and 588 cm^{-1} were due to stretching vibrations of aromatic N−H from phenolic groups and C−O−C from ester groups, respectively.[65,66] The prominent peaks at 1107 and 812 cm^{-1} were exhibited due to the presence of Cu−O and Zn−O bonds of metal biomolecules, which is in alignment with previously reported results.[50,67] The FT-IR spectra demonstrated that ZC NPs might be reduced and stabilized due to the interaction of OH and C═O residues of the phenolic compounds. Since OH and C═O residues have a great ability to bond with metal by coating their surface and inhibiting aggregation, which are essential for stabilization.[65]

3.2.4. TGA Analysis. Thermogravimetric analysis was also performed to confirm the presence of biomolecules on the surface of ZC NPs, which are used as capping and reducing agents, as illustrated in Figure 6. The DTA thermogram revealed four (two exothermic and two endothermic) distinct peaks in the temperature range of 35 to 800 °C. The endothermic peaks at 44.07 and 274.01 °C correspond to weight losses of 5.23 and 21.39% in the TGA curve. The exothermic peaks at 199.78 and 411.87 °C observed are linked with the 4.49 and 19.05% weight losses in the TGA curve. The first weight loss (5.23%) observed is associated with physically adsorbed water molecules on the surface of ZC NPs. The

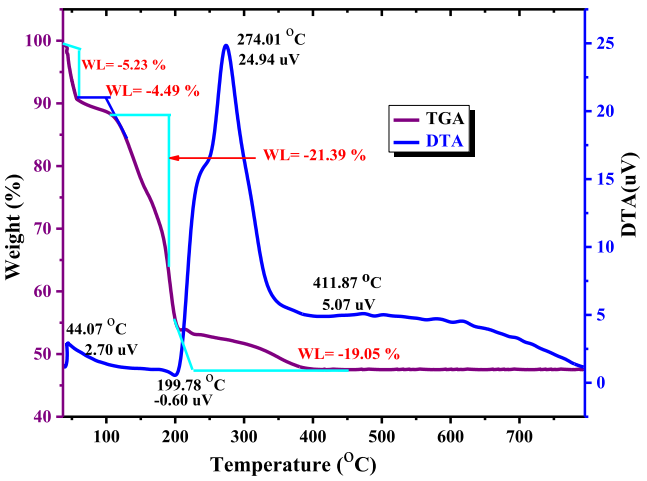

Figure 6. TGA/DTA thermogram of the biosynthesized ZC NPs.

second weight reduction on the thermogram was found to be 4.49%, which is due to the degradation of chemically adsorbed hydroxide molecules and the desorption of some biomolecules from the surfaces of ZC NPs. The third and fourth weight losses of (21.39% and 19.05%) observed were also due to the desorption of biomolecules that strongly bind with nanoparticles and which were involved in the preparation of ZC NPs.[68] As a result, phenolic compounds such as polyphenols, alkaloids, and flavonoids are expected to be present in the LEAA, which are responsible for the reduction and stabilization of ZC NPs, as previously mentioned in the FTIR study (Figure 5).[36,69]

3.2.5. SEM Analysis. The surface morphology, structure, and composition of the biosynthesized ZC NPs were characterized using scanning electron microscopy with energy-dispersive X-ray spectroscopic (SEM−EDX) techniques. As shown in (Figure 7a,b), SEM images of ZC NPs at low and high resolution were found to be nearly spherical. Furthermore, the particles are dispersed across the surface more uniformly with a low level of agglomeration/clustered forms, and that is associated with the presence of biomolecules from LEAA.

The elemental composition of the biosynthesized ZC NPs was analyzed by energy-dispersive X-ray (EDX) techniques. The formation and features of the synthesized nanomaterials are linked to the existence of characteristic peaks in the EDX spectrum. Figure 7c shows an EDX spectrum of biosynthesized ZC NPs at 0.5, 0.8, and 1 keV for the weight percent of oxygen, copper, and zinc, respectively, which is in agreement with previous studies.[32,70] The smaller peaks were also revealed at 8.2 and 9 keV for the weight percent of copper and 8.8 and 9.7 keV for the weight percent of zinc. These verified the production of crystalline bimetallic ZnO−CuO (ZC) NPs with weight percentages of 39.35, 27.42, and 26.75 for Zn, Cu, and O, respectively. The smaller peaks at 2.5 and 3.5 keV were shown weight percentages of 4.27 and 2.21 for nitrogen and carbon, respectively, which may be due to the biomolecules bound to the surface of ZC NPs. This EDX spectrum finding also confirmed the successful preparation of ZC NPs synthesized using LEAA.

3.2.6. TEM−HRTEM−SAED Analysis. The morphology, particle size, and crystallinity of ZC NPs were further characterized by TEM−HRTEM−SAED techniques. As displayed in Figure 8a,b, the as-synthesized ZC NPs have nearly spherical morphology with particle sizes ranges from 5

https://doi.org/10.1021/acsomega.3c01814
ACS Omega 2023, 8, 41039−41053

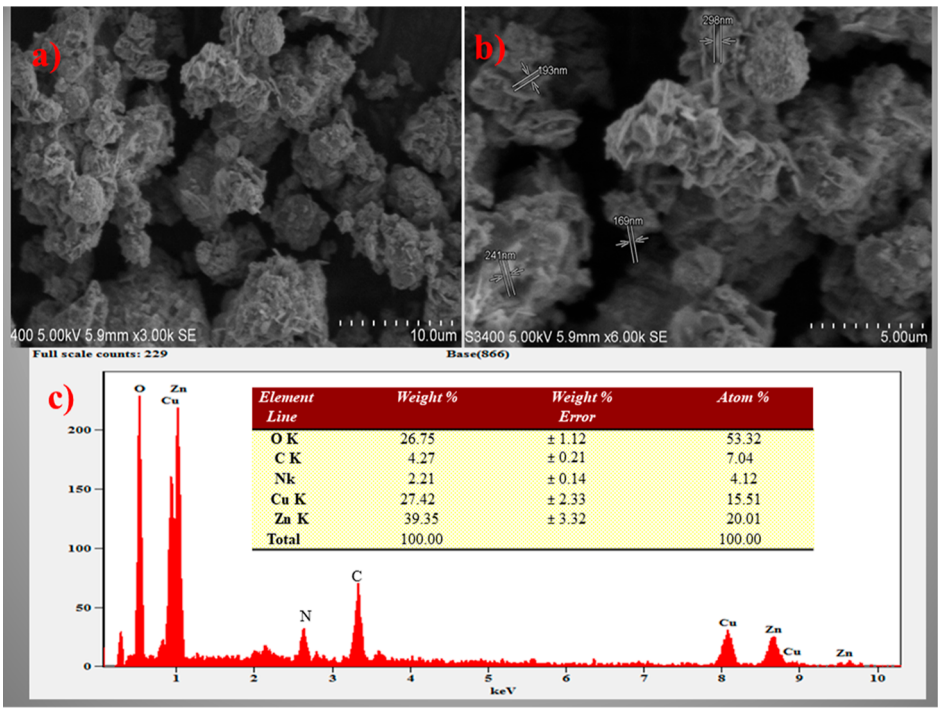

Figure 7. SEM micrographs of ZC NPs with (a) low, (b) high resolution, and (c) EDX spectrum.

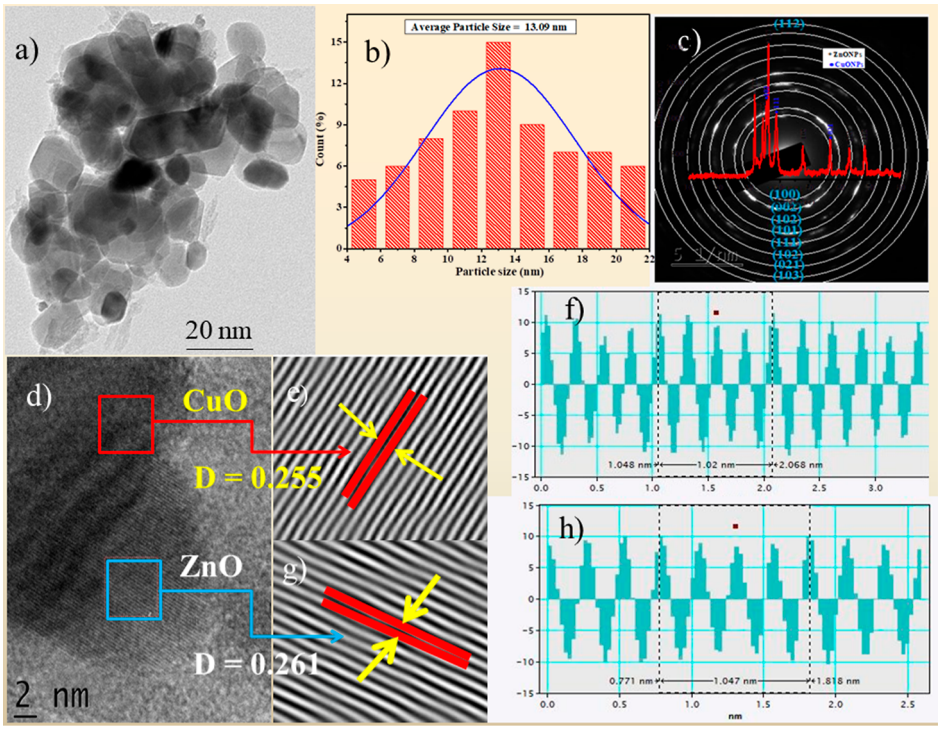

Figure 8. TEM images of ZC NPs (a) at 20 nm, (b) histogram of particle size distribution (c), SAED pattern, (d) HRTEM at 2 nm, (e) IFFT patterns with *d*-spacing of CuO, and (f) IFFT patterns with *d*-spacing of ZnO NPs, (g) profile of IFFT of CuO with *d*-spacing distance, and (h) profile of IFFT of ZnO with *d*-spacing distance.

to 22 nm. The average particle size of ZC NPs is approximately 13.09 nm, as determined by ImageJ software analysis. The presence of small particles with a size of 5 nm demonstrates the effectiveness of biomolecules from the LEAA as capping and stabilizing agents.

The eight major circular concentric circles on the SAED pattern (Figure 8c) correspond to specific crystal planes of ZC NPs as observed in XRD measurements (Figure 3). The eight most noticeable patterns found in the XRD measurements were also denoted by colored concentric circles on the SAED pattern that can be correlated to the (100), (002), (102), (111), (102), (021), (103), and (112) crystal planes (Figure 3). The ringed concentric circles of the SAED pattern revealed the fabrication of polycrystalline ZC NPs. The average *d*-space

https://doi.org/10.1021/acsomega.3c01814
ACS Omega 2023, 8, 41039−41053

Table 2. Absorbance of FRAP of Zinc Nitrate, Copper Nitrate, ZC NPs, and Ascorbic Acid[a]

concentration (μg/mL)	absorbance FRAP of $Zn(NO_3)_2{\cdot}4H_2O$, $CuNO_3{\cdot}3H_2O$, ZC NPs, and ascorbic acid			
	$Zn(NO_3)_2{\cdot}4H_2O$	$CuNO_3{\cdot}3H_2O$	ZC NPs	ascorbic acid
12.5	0.147 ± 0.004^{c}	0.156 ± 0.012^{c}	0.542 ± 0.001^{d}	0.654 ± 0.001^{d}
25	0.152 ± 0.001^{bc}	0.163 ± 0.004^{bc}	0.884 ± 0.011^{c}	0.912 ± 0.003^{c}
50	0.176 ± 0.003^{b}	0.187 ± 0.010^{b}	1.036 ± 0.001^{bc}	1.069 ± 0.002^{bc}
100	0.192 ± 0.001^{ab}	0.195 ± 0.002^{b}	1.292 ± 0.003^{b}	1.304 ± 0.006^{b}
200	0.208 ± 0.012^{a}	0.217 ± 0.001^{a}	1.826 ± 0.000^{a}	1.845 ± 0.001^{a}

[a]Absorbance values of five individual replicates ± standard deviation. The letter(s) on the means in each column are not significantly different as per Tukey's honestly significance difference (HSD) (SPSS 20.0).

Table 3. Percentages of DPPH Radical Scavenging of Zinc Nitrate, Copper Nitrate, ZC NPs, and Ascorbic Acid[a]

concentration (μg/mL)	% scavenging activity (mean ± SD) against DPPH radical- zinc nitrate, copper nitrate, ZC NPs, and ascorbic acid			
	$Zn(NO_3)_2{\cdot}4H_2O$	$CuNO_3{\cdot}3H_2O$	ZC NPs	ascorbic acid
12.5	15.28 ± 0.04^{c}	19.57 ± 0.02^{c}	65.26 ± 0.11^{c}	63.91 ± 0.03^{c}
25	21.37 ± 0.02^{bc}	23.13 ± 0.04^{bc}	72.46 ± 0.06^{bc}	70.83 ± 0.00^{bc}
50	26.46 ± 0.03^{b}	28.07 ± 0.01b^{c}	80.62 ± 0.03^{b}	78.51 ± 0.06^{b}
100	32.22 ± 0.00^{a}	33.15 ± 0.02^{b}	89.96 ± 0.04^{ab}	87.58 ± 0.01^{ab}
200	36.28 ± 0.04^{a}	38.78 ± 0.01^{a}	95.71 ± 0.02^{a}	94.56 ± 0.11^{a}
IC_{50} (μg/mL)	1096.63	1074.92	3.28	3.78

[a]The scavenging percentages (%) are the means of five individual replicates ± the standard deviation (SD). The letter(s) on the means in each column are not significantly different, per Tukey's HSD analysis.

value of 0.255 nm displayed in (Figure 8d,e), which was computed from the profile IFFT in (Figure 8f), well corresponds with the (102) planes of the spherical Tenorite structure of CuO NPs with the (ICSD card no. 00-048-1548). *D*-space value 0.261 nm (Figure 8d,g), which was computed from the profile IFFT in (Figure 8f), is also well corresponding with the (101) planes of the hexagonal zincite structure of ZnO NPs with the (ICSD card no. 00-036-1451), and it is also in accordance with the results of XRD analysis in (Figure 3).

3.3. Biological Efficacy of ZC NPs. *3.3.1. Antioxidant Assay.* The FRAP and DPPH assays were used to assess the *in vitro* antioxidant activity of the precursor salts and ZC NPs. Various amounts (200, 100, 50, 25, and 12.5 μg/mL) of samples were prepared from their respective stock solutions (1 mg/mL). Each solution was subjected to the UV−vis spectrophotometer to measure their absorbance against ferric reducing power and DPPH radical at 700 and 517 nm, respectively. The triplicate values of outcomes were expressed as mean ± standard deviation.

3.3.1.1. FRAP Assay. The potential of reducing the ferric (Fe^{3+}) ion into its ferrous (Fe^{2+}) precursor salts and ZC NPs was known by first observing a change in color of the reaction solutions from yellow to green and then measuring the absorbance at 700 nm.[43] The ability to reduce Fe^{3+} to Fe^{2+} (ferric reducing antioxidant power) ions by donor electrons, as revealed in Table 2, was found to be in the increasing order of [$Zn(NO_3)_2{\cdot}4H_2O$ < $Cu(NO_3)_2{\cdot}3H_2O$] < ZC NPs < ascorbic acid. The computed results show that at 200 μg/mL, the biosynthesized ZC NPs and ascorbic acid have higher (1.826 ± 0.000 and 1.845 ± 0.001) ferric reducing power, and the precursor salts (0.208 ± 0.012 and 0.217 ± 0.001) have lower ferric reducing power, respectively. The strong ferric reducing power of biosynthesized ZC NPs displayed may be due to the occurrence of free charge transferring between the containing copper and zinc oxides.[71] In general, the biosynthesized ZC NPs demonstrated the significant ferric reducing antioxidant power, which is also in agreement with earlier reports.[71,72]

3.3.1.2. DPPH Assay. A DPPH assay was used to evaluate the in vitro antioxidant activity of the precursor salts and ZC NPs. The absorbance of each sample was recorded against DPPH radical at 517 nm using a UV−vis spectrophotometer. As shown in Table 3 and Figure 9 DPPH radical scavenging

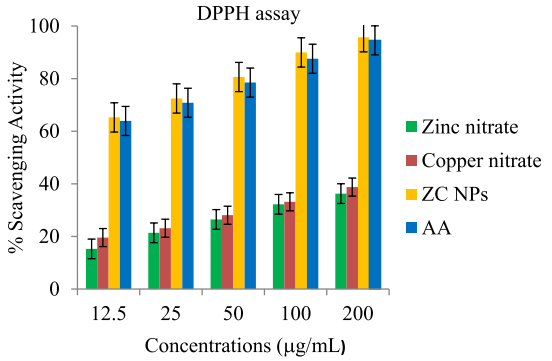

Figure 9. DPPH radical scavenging activities of zinc nitrate, copper nitrate, ZC NPs, and ascorbic acid.

activity of the samples was found to increase in a dose-dependent manner. The highest anti-DPPH scavenging potencies of precursor salts [$Zn(NO_3)_2{\cdot}4H_2O$ and $Cu(NO_3)_2{\cdot}3H_2O$] were 36.28 ± 0.04 and 38.78 ± 0.01 at 200 μg/mL, respectively. DPPH radical scavenging percentages of ZC NPs and ascorbic acid at 200 μg/mL were 95.71 ± 0.02 and 94.56 ± 0.11, respectively. The IC_{50} values of $Zn(NO_3)_2{\cdot}4H_2O$, $Cu(NO_3)_2{\cdot}3H_2O$, ZC NPs, and ascorbic acid were 1096.63, 1074.92, 3.28, and 3.78 μg/mL, respectively. The IC_{50} values of precursor salts are very large compared to those of the ZC NPs and positive control. Hence, the highest IC_{50} values of precursor salts revealed less DPPH scavenging potency and even negligible compared to ZC NPs and ascorbic acid. Likewise, the IC_{50} value of ZC NPs is smaller than the IC_{50} value of the standard drug. The lower IC_{50} value of ZC NPs indicates a stronger DPPH scavenging ability. Moreover,

https://doi.org/10.1021/acsomega.3c01814
ACS Omega 2023, 8, 41039−41053

Table 4. Inhibition Percent (%) of ZC NPs and Standard Drug against PBM and MCF7 Cell Lines on the MTT Assay[a]

conc. (μg/mL)	ZC NPs		doxorubicin	
	PBMCs	MCF7	PBMCs	MCF7
	% In.	% In.	% In.	% In.
Control	0	0	0	0
7.81	12.99 ± 0.22^{d}	25.12 ± 0.04^{d}	15.54 ± 0.02^{d}	23.94 ± 0.02^{d}
15.62	19.77 ± 0.01^{cd}	35.92 ± 0.02^{cd}	21.47 ± 0.04^{cd}	35.44 ± 0.01^{cd}
31.25	27.68 ± 0.02^{c}	51.41 ± 0.01^{c}	30.23 ± 0.01^{c}	49.76 ± 0.02^{c}
62.5	33.89 ± 0.03^{bc}	64.32 ± 0.03^{bc}	35.31 ± 0.03^{bc}	63.85 ± 0.00^{bc}
125	41.52 ± 0.00^{b}	71.12 ± 0.00^{b}	42.66 ± 0.01^{b}	70.18 ± 0.02^{b}
250	51.13 ± 0.00^{a}	81.46 ± 0.02^{ab}	53.39 ± 0.02^{ab}	79.58 ± 0.04^{ab}
500	57.91 ± 0.01^{a}	89.20 ± 0.03^{a}	60.17 ± 0.01^{a}	86.15 ± 0.03^{a}
IC50 (μg/mL)	247.15	33.12	234.67	35.94

[a]The inhibition rates in (%) are the means of seven individual replicates ± the standard deviation (SD). The letter(s) on the means in each column are not significantly different as per Tukey's HSD analysis.

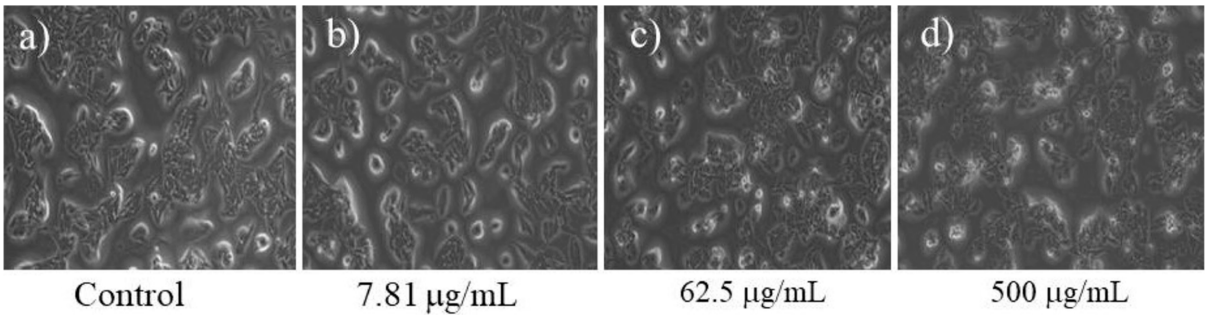

Figure 10. Cytotoxicity of ZC NPs against PBM cell lines: (a) untreated, (b) treated with 7.81, (c) 62.5, and (d) 500 μg/mL.

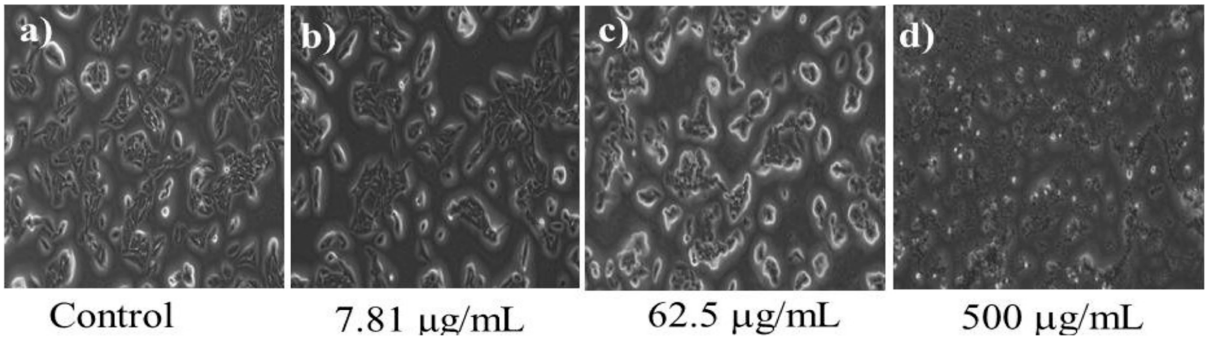

Figure 11. Cytotoxicity of ZC NPs against MCF-7 cell lines: (a) untreated, (b) treated with 7.81, (c) 62.5 μg/mL, and (d) 500 μg/mL.

bimetallic ZC NPs also showed enhanced anti-DPPH free radical scavenging activity than monometallic CuO and ZnO NPs, which were reported in previous works.[36,73] These may be due to the occurrence of free charge transferring from the containing CuO and ZnO NPs to the DPPH radical.[74] Therefore, the biosynthesized ZC NPs from the *A. abyssinica* extract can be a promising antioxidant drug in oxidative stress emerging ailments.

3.3.2. Cytotoxicity and Anticancer Activity. *In vitro* cytotoxicity and anticancer activity of biosynthesized ZC NPs and Doxorubicin (a standard chemotropic drug) were tested on peripheral blood mononuclear (PBM) and breast cancer (MCF-7) cell lines by using an MTT assay.

3.3.2.1. Cytotoxicity Test. The cytotoxicity test of doxorubicin and ZC NPs on human normal cell lines was thought to be the initial step in determining the safety of these products.[75] The cytotoxic properties of the ZC NPs on PBM cell lines at different concentrations (7.81, 15.62, 31.25, 62.5, 125, 250, and 500 μg/mL) were evaluated, as shown in Table 4 and Figures 10 and 12). The obtained result corroborated

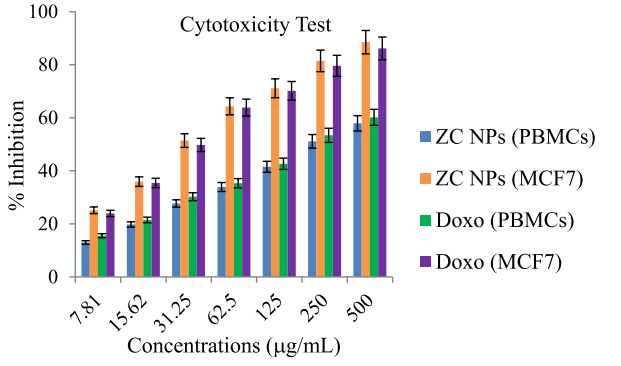

Figure 12. Cytotoxicity of ZC NPs and doxorubicin against PBM and MCF-7 cell lines, respectively.

https://doi.org/10.1021/acsomega.3c01814
ACS Omega 2023, 8, 41039−41053

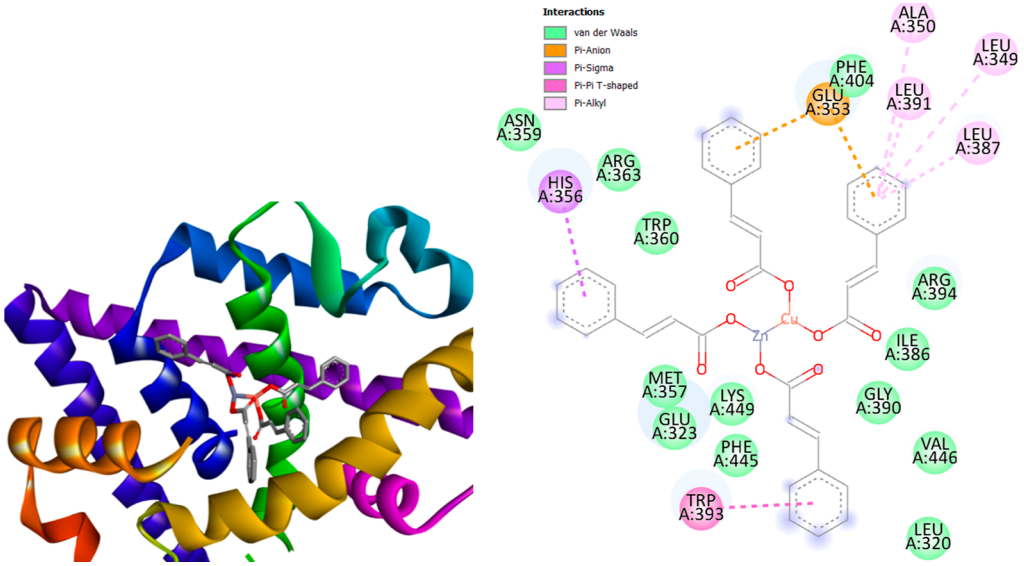

Figure 13. 3D (left) and 2D (right) pictorial representations of the binding interactions of ZC NPs against estrogen receptor alpha (ERα; PDB: 5GS4).

Table 5. Molecular Docking Scores and the Corresponding Prominent Residual Amino Acid Interactions of ZC NPs and Doxorubicin against Estrogen Receptor Alpha (ERα; PDB: 5GS4)

samples	lowest binding energy (kcal/mol)	inhibition constant (K_i)	H-bonding	π-sigma/π-alkyl	van der Waals
ZC NPs	−8.50	0.59 μM		Glu-353, His-356, Leu-391, Trp-393	Arg-363, Trp-360, Met357, Lys-449
doxorubicin	−7.54	2.99 μM	Glu-353, Arg-394, Trp-393, Glu-323	Met-357, Trp-360, Ile-386, His-356	Gly-390, Leu-387, Lys-449

that *a* % inhibition of ZC NPs against PBM cell lines was 57.91 ± 0.01 at the highest concentration at 500 μg/mL. Doxorubicin (a standard drug) has shown the % inhibition value of 60.17 ± 0.01 at 500 μg/mL against PBMC cell lines. When compared with the standard drug, ZC NPs have shown slightly better cytotoxicity against PBM cell lines with similar concentrations. The IC_{50} of ZC NPs and Doxorubicin were 247.15 and 234.67 μg/mL, respectively. The obtained high value of $IC_{50,}$ which is ≥90 μg/mL, confirmed that ZC NPs are noncytotoxic to the PBM cell lines.[76] This may be due to the synthesis of nanoparticles from biological precursors and more physiologically functioning (Cu^{2+} and Zn^{2+}) metal ions, which make them biocompatible and less cytotoxic to normal cells.

3.3.2.2. Anticancer Activity Test. The anticancer activity of ZC NPs at various concentrations (7.81, 15.62, 31.25, 62.5, 125, 250, and 500 g/mL) was evaluated against MCF-7 cell lines. Table 4 and Figures 11 & 12) results showed that, in a time-dependent manner, cell viability was shown to decline when concentrations of ZC NPs and doxorubicin increased. ZC NPs and doxorubicin have revealed the highest percent (%) inhibition of 89.20 ± 0.03 and 86.15 ± 0.03 at 500 μg/mL against MCF-7, respectively. Their respective IC50 values of ZC NPs and doxorubicin were 33.12 and 35.94 μg/mL, respectively. The lower IC50 value of ZC NPs also confirms its higher anticancer potency compared with the standard drug. Microscopic images presented in Figure 11a−d demonstrate the cell morphology of untreated MCF-7 cells and those treated with 7.81, 62.5, and 500 μg/mL, respectively. After treatment with 7.81, 62.5, and 500 μg/mL ZC NPs, the cells displayed altered morphology and reduced cell density. Moreover, at 500 μg/mL, the epithelial morphology of MCF-7 was damaged and displayed very low cell density. Generally, the obtained microscopic and cell viability results demonstrated the significant anticancer potency of ZC NPs. The findings of this study are also well corroborated by previous studies that were reported in other works.[77,78]

The proposed mechanism of action of ZC NPs as an anticancer agent could be either van der Waals interaction with different amino acids of protein targets of breast cancer, as discussed in (Figure 13). In addition to this, it could also be the apoptotic cellular death induced due to the generation of ROS in the cellular environment and which results in oxidative stress on the cancer cells. Furthermore, it might cause DNA binding as a result of an electrochemical interaction between a positive charge on the ZC NPs and certain negative charges on the surface of the DNA of cancer cells. Moreover, ZC NPs demonstrated greater cytotoxicity in the MCF-7 cell line due to their compact size, improved surface-to-volume ratio, and richer electrochemical characteristics.[77,79] Therefore, ZC NPs can be an effective therapeutic agent in cancer chemotherapy, particularly in breast cancer ailments, and hence probably will be a promising candidate for the development and design of anticancer drugs.

3.3.3. Molecular Docking Study. Evaluations of the interaction efficiency and the binding affinity of molecules with specific targets are among the important factors in drug design and development. The interactions of ZC NPs and doxorubicin were investigated against estrogen receptor alpha (ERα; PDB: 5GS4) using AutoDock 4.2 (MGL tools 1.5.7) with a molecular docking database. Estrogen receptor (ERα) is the major clinical biomarker used to subtype breast cancers.[11,48] The estrogen receptor α (ERα) plays an

https://doi.org/10.1021/acsomega.3c01814
ACS Omega 2023, 8, 41039−41053

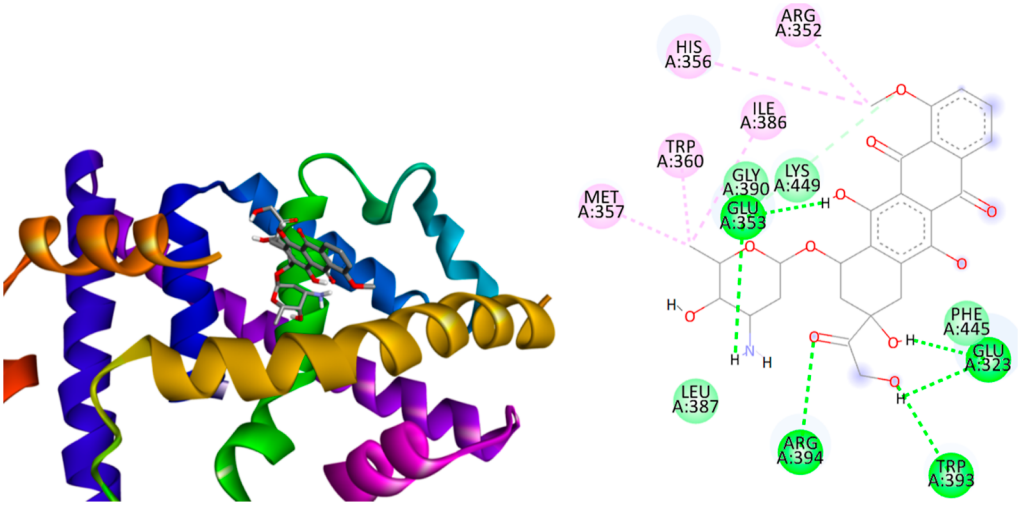

Figure 14. 3D (left) and 2D (right) pictorial representations of the binding interactions of doxorubicin against estrogen receptor alpha (ERα; PDB: 5GS4).

important role in the development and progression of hormonal-dependent type breast cancer.[80]

The biosynthesized ZC NPs (Table 5 and Figure 13) have revealed a remarkable binding affinity through van der Waals and π-Sigma/π-Alkyl interactions within the active sites of estrogen receptors (ERα) through key amino acids like Glu-353, His-356, Leu-391, Trp-393, Arg-363, Trp-360, Met-357, and Lys-449. Doxorubicin (Table 5 and Figure 14) has shown H-bonding, π-Sigma/π-Alkyl, and van der Waals interactions within Glu-353, Arg-394, Trp-393, Glu-323, Met-357, Trp-360, Ile-386, His-356, Gly-390, Leu-387, and Lys-449 amino acid residues. Both biosynthesized ZC NPs and the standard drug have shown strong interactions with active sites of amino acid residues of estrogen receptors (ERα). These strong binding with amino acids of estrogen receptors (ERα) is important to inhibit the proliferation rates of breast cancer cells.[49] However, the binding domain of ZC NPs (−8.50 kcal/mol) was slightly better than the standard drug doxorubicin, which was −7.54 kcal/mol. These demonstrate the biosynthesized ZC NPs will have strong interactions with estrogen receptor alpha (ERα; PDB: 5GS4) than the standard drug. Moreover, the molecular docking interactions are also correlated with the experimental results presented in Table 4 and confirmed its anticancer efficacy in MCF-7 cell lines. Consequently, the biosynthesized ZC NPs can be a promising anticancer drug candidate, particularly for breast cancer ailments.

4. CONCLUSIONS

This study reports an ecofriendly, one-pot approach synthesized bimetallic ZC NPs from the leaf extract of *A. abyssinica* for the first time. Ultrapure, iso-morphological, and spherical ZC NPs with an average particle size below 14 nm were prepared and confirmed with UV−vis, FTIR, TGA, XRD, SEM, EDX, and TEM techniques. ZC NPs have exhibited remarkable antioxidant potential, as investigated through FRAP and DPPH assays. As the results revealed, ZC NPs have strong ferric-ion reducing power (1.826 ± 0.000) and DPPH radical scavenging (95.71 ± 0.02%) with an IC50 value of 3.28 μg/mL. Moreover, the higher (%) inhibition (89.20 ± 0.03), small IC50 value (33.12 μg/mL), and the microscopic observation with very low cell density confirmed the anticancer potency of ZC NPs against MCF-7 cell lines. Further, ZC NPs have also exhibited strong binding affinity against estrogen receptor alpha (ERα) through in silico molecular docking simulations. Overall, the mixed-phase biosynthesized ZC NPs have exhibited multifunctional biological activities. As a result, ZC NPs can be used as potential biosafe antioxidant and anticancer drug candidates, particularly for breast cancer ailments. However, *in vivo* antioxidant and anticancer potency of ZC NPs are recommended in different animal models.

■ ASSOCIATED CONTENT

Data Availability Statement

The data used to support the findings of the study are available from the corresponding author upon responsible request.

■ AUTHOR INFORMATION

Corresponding Authors

Temesgen Achamo Orshiso − *Department of Applied Chemistry, School of Applied Natural Sciences, Adama Science and Technology University, Adama 1888, Ethiopia;* orcid.org/0000-0002-1491-5928; Email: temachamo2000@gmail.com

Enyew Amare Zereffa − *Department of Applied Chemistry, School of Applied Natural Sciences, Adama Science and Technology University, Adama 1888, Ethiopia;* Email: enyewama@yahoo.com

H. C. Ananda Murthy − *Department of Applied Chemistry, School of Applied Natural Sciences, Adama Science and Technology University, Adama 1888, Ethiopia; Department of Prosthodontics, Saveetha Dental College & Hospital, Saveetha Institute of Medical and Technical Science (SIMAT), Saveetha University, Chennai 600077 Tamil Nadu, India;* orcid.org/0000-0002-2361-086X; Email: Murthy-anandkps350@gmail.com

Taye B. Demissie − *Department of Chemistry, University of Botswana, Gaborone 0022, Botswana;* orcid.org/0000-0001-8735-4933; Email: demissiet@ub.ac.bw

Authors

Onkar Pardeshi − *Department of Electronics, KKHA Arts, SMGL Commerce and SPHJ Science College, Savitribai*

https://doi.org/10.1021/acsomega.3c01814
ACS Omega 2023, 8, 41039−41053

Phule Pune University, Chandwad 423 101 Maharashtra, India

Lata S. Avhad − *Department of Chemistry, Karmaveer Shantarambapu Kondaji Wavare Arts, Science & Commerce College, Savitribai Phule Pune University, Nashik 422008 Maharashtra, India*

Suresh Ghotekar − *Faculty of Allied Health Sciences, Chettinad Hospital and Research Institute, Chettinad Academy of Research and Education, Kelambakkam 603103 Tamil Nadu, India;* orcid.org/0000-0001-7679-8344

Complete contact information is available at: https://pubs.acs.org/10.1021/acsomega.3c01814

Author Contributions

Conceptualization, sample collection, investigation, evaluation, analysis, and initial draft preparation were conducted by Temesgen Achamo Orshiso. Categorization, supervision, validation, correction, and rewriting were handled by Enyew Amare Zereffa and H. C. Ananda Murthy. Analysis, validations, molecular docking calculations, and editing of the manuscript were computed by Taye B. Demissie, Onkar Pardeshi, Lata S. Avhad, and Suresh Ghotekar.

Notes

The authors declare no competing financial interest.
Ethical approval: This study did not include human participants or animals.

■ ACKNOWLEDGMENTS

The authors would like to thank Adama Science and Technology University and Haramaya University for technical and material support.

■ REFERENCES

(1) (a) Anastasopoulos, N.-A.; Charchanti, A. V.; Barbouti, A.; Mastoridou, E. M.; Goussia, A. C.; Karampa, A. D.; Christodoulou, D.; Glantzounis, G. K. The Role of Oxidative Stress and Cellular Senescence in the Pathogenesis of Metabolic Associated Fatty Liver Disease and Related Hepatocellular Carcinoma. *Antioxidants* **2023**, *12* (6), 1269. (b) Deo, S.; Sharma, J.; Kumar, S. GLOBOCAN 2020 report on global cancer burden: challenges and opportunities for surgical oncologists. *Ann. Surg. Oncol.* **2022**, *29* (11), 6497−6500.

(2) (a) Sung, H.; Ferlay, J.; Siegel, R. L.; Laversanne, M.; Soerjomataram, I.; Jemal, A.; Bray, F. Global cancer statistics 2020: GLOBOCAN estimates of incidence and mortality worldwide for 36 cancers in 185 countries. *Ca-Cancer J. Clin.* **2021**, *71* (3), 209−249. (b) Zuo, L.; Prather, E. R.; Stetskiv, M.; Garrison, D. E.; Meade, J. R.; Peace, T. I.; Zhou, T. Inflammaging and oxidative stress in human diseases: from molecular mechanisms to novel treatments. *Int. J. Mol. Sci.* **2019**, *20* (18), 4472.

(3) Papaccio, F.; D'Arino, A.; Caputo, S.; Bellei, B. Focus on the contribution of oxidative stress in skin aging. *Antioxidants* **2022**, *11* (6), 1121.

(4) Mokoena, D.; George, B.; Abrahamse, H. The Role of Cannabis Species on Oxidative Stress in Cancer Cells. In *Handbook of Oxidative Stress in Cancer: Therapeutic Aspects*; Springer, 2022, pp 1−14.

(5) (a) Bayón-Cordero, L.; Alkorta, I.; Arana, L. Application of solid lipid nanoparticles to improve the efficiency of anticancer drugs. *Nanomaterials* **2019**, *9* (3), 474. (b) Dallavalle, S.; Dobričić, V.; Lazzarato, L.; Gazzano, E.; Machuqueiro, M.; Pajeva, I.; Tsakovska, I.; Zidar, N.; Fruttero, R. Improvement of conventional anti-cancer drugs as new tools against multidrug resistant tumors. *Drug Resistance Updates* **2020**, *50*, 100682. (c) Garcia-Oliveira, P.; Otero, P.; Pereira, A. G.; Chamorro, F.; Carpena, M.; Echave, J.; Fraga-Corral, M.; Simal-Gandara, J.; Prieto, M. A. Status and challenges of plant-anticancer compounds in cancer treatment. *Pharmaceuticals* **2021**, *14* (2), 157.

(6) (a) Vona, R.; Pallotta, L.; Cappelletti, M.; Severi, C.; Matarrese, P. The impact of oxidative stress in human pathology: Focus on gastrointestinal disorders. *Antioxidants* **2021**, *10* (2), 201. (b) Albuquerque, B. R.; Heleno, S. A.; Oliveira, M. B. P.; Barros, L.; Ferreira, I. C. Phenolic compounds: Current industrial applications, limitations and future challenges. *Food Funct.* **2021**, *12* (1), 14−29.

(7) (a) Augustine, R.; Hasan, A. Emerging applications of biocompatible phytosynthesized metal/metal oxide nanoparticles in healthcare. *J. Drug Delivery Sci. Technol.* **2020**, *56*, 101516. (b) Abdelghany, T. M.; Al-Rajhi, A. M.; Yahya, R.; Bakri, M. M.; Al Abboud, M. A.; Yahya, R.; Qanash, H.; Bazaid, A. S.; Salem, S. S. Phytofabrication of zinc oxide nanoparticles with advanced characterization and its antioxidant, anticancer, and antimicrobial activity against pathogenic microorganisms. *Biomass Convers. Biorefin.* **2023**, *13* (1), 417−430.

(8) Kannan, K.; Radhika, D.; Sadasivuni, K. K.; Reddy, K. R.; Raghu, A. V. Nanostructured metal oxides and its hybrids for photocatalytic and biomedical applications. *Adv. Colloid Interface Sci.* **2020**, *281*, 102178.

(9) Chouke, P. B.; Shrirame, T.; Potbhare, A. K.; Mondal, A.; Chaudhary, A. R.; Mondal, S.; Thakare, S. R.; Nepovimova, E.; Valis, M.; Kuca, K.; et al. Bioinspired metal/metal oxide nanoparticles: A road map to potential applications. *Mater. Today Adv.* **2022**, *16*, 100314.

(10) (a) Ehsan, M.; Waheed, A.; Ullah, A.; Kazmi, A.; Ali, A.; Raja, N. I.; Mashwani, Z.-u.-R.; Sultana, T.; Mustafa, N.; Ikram, M.; et al. Plant-Based Bimetallic Silver-Zinc Oxide Nanoparticles: A Comprehensive Perspective of Synthesis, Biomedical Applications, and Future Trends. *BioMed Res. Int.* **2022**, *2022*, 1−20. (b) Yusefi, M.; Shameli, K.; Ali, R. R.; Pang, S.-W.; Teow, S.-Y. Evaluating anticancer activity of plant-mediated synthesized iron oxide nanoparticles using Punica granatum fruit peel extract. *J. Mol. Struct.* **2020**, *1204*, 127539. (c) Hassan, H. F. H.; Mansour, A. M.; Abo-Youssef, A. M. H.; Elsadek, B. E.; Messiha, B. A. S. Zinc oxide nanoparticles as a novel anticancer approach; in vitro and in vivo evidence. *Clin. Exp. Pharmacol. Physiol.* **2017**, *44* (2), 235−243.

(11) Anza, M.; Endale, M.; Cardona, L.; Cortes, D.; Eswaramoorthy, R.; Cabedo, N.; Abarca, B.; Zueco, J.; Rico, H.; Domingo-Ortí, I. Cytotoxicity, antimicrobial activity, molecular docking, drug likeness and DFT analysis of benzo [c] phenanthridine alkaloids from roots of Zanthoxylum chalybeum. *Biointerface Res. Appl. Chem.* **2021**, *12* (2), 1569−1586.

(12) Sathiyavimal, S.; F Durán-Lara, E.; Vasantharaj, S.; Saravanan, M.; Sabour, A.; Alshiekheid, M.; Lan Chi, N. T.; Brindhadevi, K.; Pugazhendhi, A. Green synthesis of copper oxide nanoparticles using Abutilon indicum leaves extract and their evaluation of antibacterial, anticancer in human A549 lung and MDA-MB-231 breast cancer cells. *Food Chem. Toxicol.* **2022**, *168*, 113330.

(13) (a) Shahzadi, I.; Islam, M.; Saeed, H.; Shahzadi, A.; Haider, J.; Haider, A.; Imran, M.; Rathore, H. A.; Ul-Hamid, A.; Nabgan, W.; et al. Facile synthesis of copolymerized cellulose grafted hydrogel doped calcium oxide nanocomposites with improved antioxidant activity for anti-arthritic and controlled release of doxorubicin for anticancer evaluation. *Int. J. Biol. Macromol.* **2023**, *235*, 123874. (b) Ravichandran, S.; Radhakrishnan, J.; Sengodan, P.; Rajendran, R.; Ramalingam, R.; Arunachalam, K. D. Bio synthesis of Zinc oxide nanoparticles using Clerodendrum phlomidis extract for antibacterial, anticancer, antioxidant and photocatalytic studies. *J. Mater. Sci.: Mater. Electron.* **2022**, *33* (14), 11455−11466. (c) Kala, K.; Jeyalakshmi, M.; Mohandoss, S.; Chandrasekaran, R. Evolution of anticancer, antioxidant and photocatalytic activities of biosynthesized MnO2 nanoparticles using aqueous extract of Sida acuta. *Surf. Interfaces* **2023**, *40*, 103136.

(14) Jha, S.; Rani, R.; Singh, S. Biogenic Zinc Oxide Nanoparticles and Their Biomedical Applications: A Review. *J. Inorg. Organomet. Polym. Mater.* **2023**, *33*, 1437−1452.

(15) Talebian, S.; Shahnavaz, B.; Nejabat, M.; Abolhassani, Y.; Rassouli, F. B. Bacterial-mediated synthesis and characterization of copper oxide nanoparticles with antibacterial, antioxidant, and anticancer potentials. *Front. Bioeng. Biotechnol.* **2023**, *11*, 1140010.
(16) Adeyemi, J. O.; Onwudiwe, D. C.; Oyedeji, A. O. Biogenic synthesis of CuO, ZnO, and CuO-ZnO nanoparticles using leaf extracts of Dovyalis caffra and their biological properties. *Molecules* **2022**, *27* (10), 3206.
(17) Khalid, A. D.; Ur-Rehman, N.; Tariq, G. H.; Ullah, S.; Buzdar, S. A.; Iqbal, S. S.; Sher, E. K.; Alsaiari, N. S.; Hickman, G. J.; Sher, F. Functional bioinspired nanocomposites for anticancer activity with generation of reactive oxygen species. *Chemosphere* **2023**, *310*, 136885.
(18) (a) Meer, B.; Andleeb, A.; Iqbal, J.; Ashraf, H.; Meer, K.; Ali, J. S.; Drouet, S.; Anjum, S.; Mehmood, A.; Khan, T.; et al. Bio-Assisted Synthesis and Characterization of Zinc Oxide Nanoparticles from Lepidium Sativum and Their Potent Antioxidant, Antibacterial and Anticancer Activities. *Biomolecules* **2022**, *12* (6), 855. (b) Hadi, A. J.; Nayef, U. M.; Mutlak, F. A.-H.; Jabir, M. S. Laser-ablated zinc oxide nanoparticles and evaluation of their antibacterial and anticancer activity against an ovarian cancer cell line: in vitro study. *Plasmonics* **2023**, 1−11.
(19) Rani, N.; Rawat, K.; Saini, M.; Yadav, S.; Shrivastava, A.; Saini, K.; Maity, D. Azadirachta indica leaf extract mediated biosynthesized rod-shaped zinc oxide nanoparticles for in vitro lung cancer treatment. *Mater. Sci. Eng. B* **2022**, *284*, 115851.
(20) Ahamed, M.; Lateef, R.; Khan, M. A. M.; Rajanahalli, P.; Akhtar, M. J. Biosynthesis, Characterization, and Augmented Anticancer Activity of ZrO2 Doped ZnO/rGO Nanocomposite. *J. Funct. Biomater.* **2023**, *14* (1), 38.
(21) Mousa, A. B.; Moawad, R.; Abdallah, Y.; Abdel-Rasheed, M.; Zaher, A. M. A. Zinc Oxide Nanoparticles Promise Anticancer and Antibacterial Activity in Ovarian Cancer. *Pharm. Res.* **2023**, 1−10.
(22) Efati, Z.; Shahangian, S. S.; Darroudi, M.; Amiri, H.; Hashemy, S. I.; Aghamaali, M. R. Green chemistry synthesized zinc oxide nanoparticles in Lepidium sativum L. seed extract and evaluation of their anticancer activity in human colorectal cancer cells. *Ceram. Int.* **2023**, *49*, 32568−32576.
(23) (a) Naser, S. S.; Ghosh, B.; Simnani, F. Z.; Singh, D.; Choudhury, A.; Nandi, A.; Sinha, A.; Jha, E.; Panda, P. K.; Suar, M.; et al. Emerging Trends in the Application of Green Synthesized Biocompatible ZnO Nanoparticles for Translational Paradigm in Cancer Therapy. *J. Nanotheranostics* **2023**, *4* (3), 248−279. (b) Aboul-Soud, M. A.; Siddique, R.; Fozia, F.; Ullah, A.; Rashid, Y.; Ahmad, I.; Zaghloul, N. S.; Al-Rejaie, S. S.; Mohany, M. Antiplatelet, cytotoxic activities and characterization of green-synthesized zinc oxide nanoparticles using aqueous extract of Nephrolepis exaltata. *Environ. Sci. Pollut. Res.* **2023**, *30*, 73870−73880.
(24) Dolati, M.; Tafvizi, F.; Salehipour, M.; Komeili Movahed, T.; Jafari, P. Biogenic copper oxide nanoparticles from Bacillus coagulans induced reactive oxygen species generation and apoptotic and anti-metastatic activities in breast cancer cells. *Sci. Rep.* **2023**, *13* (1), 3256.
(25) Younas, M.; Zubair, M.; Rizwan, M.; Khan, M. A.; Hussaini, K. M.; Mumtaz, R.; Azeem, M.; Abbas, T.; Irshad, M. A.; Ali, S. Synthesis and characterization of cerium, silver and copper oxide nanoparticles and their anticancer potential of hepatocellular carcinoma HepG2 cancer cells. *J. Mol. Struct.* **2023**, *1288*, 135756.
(26) Doman, K. M.; Gharieb, M. M.; Abd El-Monem, A. M.; Morsi, H. H. Synthesis of silver and copper nanoparticle using Spirulina platensis and evaluation of their anticancer activity. *Int. J. Environ. Health Res.* **2023**, 1−13.
(27) Mohammad, M. S.; Shyam, P. Structural Analysis of Biogenic Copper Oxide Nanoparticles, and their Bio-Activity Assessment. *BioNanoSci.* **2023**.
(28) Sathiyavimal, S.; Vasantharaj, S.; Kaliannan, T.; Garalleh, H. A.; Garaleh, M.; Brindhadevi, K.; Chi, N. T. L.; Sharma, A.; Pugazhendhi, A. Bio-functionalized copper oxide/chitosan nanocomposite using Sida cordifolia and their efficient properties of antibacterial, anticancer activity against on breast and lung cancer cell lines. *Environ. Res.* **2023**, *218*, 114986.
(29) (a) Krishnamoorthy, N.; Sivasankarapillai, V. S.; Natarajan, V. K.; Eldesoky, G. E.; Wabaidur, S. M.; Eswaran, M.; Dhanusuraman, R. Biocidal activity of ZnO NPs against pathogens and antioxidant activity-a greener approach by Citrus hystrix leaf extract as bio-reductant. *Biochem. Eng. J.* **2023**, *192*, 108818. (b) Ghaffar, S.; Abbas, A.; Naeem-ul-Hassan, M.; Assad, N.; Sher, M.; Ullah, S.; Alhazmi, H. A.; Najmi, A.; Zoghebi, K.; Al Bratty, M.; et al. Improved Photocatalytic and Antioxidant Activity of Olive Fruit Extract-Mediated ZnO Nanoparticles. *Antioxidants* **2023**, *12* (6), 1201.
(30) Shalaby, E. A.; Shanab, S. M.; El-Raheem, W. M. A.; Hanafy, E. A. Biological activities and antioxidant potential of different biosynthesized nanoparticles of Moringa oleifera. *Sci. Rep.* **2022**, *12* (1), 18400.
(31) (a) Basavegowda, N.; Baek, K.-H. Multimetallic nanoparticles as alternative antimicrobial agents: challenges and perspectives. *Molecules* **2021**, *26* (4), 912. (b) Iribarnegaray, V.; Navarro, N.; Robino, L.; Zunino, P.; Morales, J.; Scavone, P. Magnesium-doped zinc oxide nanoparticles alter biofilm formation of Proteus mirabilis. *Nanomedicine* **2019**, *14* (12), 1551−1564.
(32) Merugu, R.; Gothalwal, R.; Kaushik Deshpande, P.; De Mandal, S.; Padala, G.; Latha Chitturi, K. Synthesis of Ag/Cu and Cu/Zn bimetallic nanoparticles using toddy palm: Investigations of their antitumor, antioxidant and antibacterial activities. *Mater. Today: Proc.* **2021**, *44*, 99−105.
(33) (a) Panahi, A.; Monsef, R.; Imran, M. K.; Mahdi, A. A.; Kadhim Ruhaima, A. A.; Salavati-Niasari, M. TmVO4/Fe2O3 nanocomposites: sonochemical synthesis, characterization, and investigation of photocatalytic activity. *Int. J. Hydrogen Energy* **2023**, *48* (10), 3916−3930. (b) Amiri, M.; Eskandari, K.; Salavati-Niasari, M. Magnetically retrievable ferrite nanoparticles in the catalysis application. *Adv. Colloid Interface Sci.* **2019**, *271*, 101982.
(34) (a) Eid, A. M.; Fouda, A.; Hassan, S. E.-D.; Hamza, M. F.; Alharbi, N. K.; Elkelish, A.; Alharthi, A.; Salem, W. M. Plant-Based Copper Oxide Nanoparticles; Biosynthesis, Characterization, Antibacterial Activity, Tanning Wastewater Treatment, and Heavy Metals Sorption. *Catalysts* **2023**, *13* (2), 348. (b) Mahdavi, B.; Saneei, S.; Qorbani, M.; Zhaleh, M.; Zangeneh, A.; Zangeneh, M. M.; Pirabbasi, E.; Abbasi, N.; Ghaneialvar, H. Ziziphora clinopodioides Lam leaves aqueous extract mediated synthesis of zinc nanoparticles and their antibacterial, antifungal, cytotoxicity, antioxidant, and cutaneous wound healing properties under in vitro and in vivo conditions. *Appl. Organomet. Chem.* **2019**, *33* (11), No. e5164. (c) Zhang, D.; Ma, X.-l.; Gu, Y.; Huang, H.; Zhang, G.-w. Green synthesis of metallic nanoparticles and their potential applications to treat cancer. *Front. Chem.* **2020**, *8*, 799.
(35) Aman, M.; Asfaw, Z.; Dalle, G. *Medicinal Plants Used for Treating Human and Livestock Ailments in Tiyo District, Arsi Zone of Oromia, Ethiopia*, 2020.
(36) Achamo, T.; Zereffa, E. A.; Murthy, H. C. A.; Ramachandran, V. P.; Balachandran, R. Phyto-mediated synthesis of copper oxide nanoparticles using Artemisia abyssinica leaf extract and its antioxidant, antimicrobial and DNA binding activities. *Green Chem. Lett. Rev.* **2022**, *15* (3), 598−614.
(37) Barui, A. K.; Das, S.; Patra, C. R. Biomedical applications of green-synthesized metal nanoparticles using polysaccharides. In *Functional Polysaccharides for Biomedical Applications*; Elsevier, 2019; pp 329−355.
(38) Majeed, M.; Hakeem, K. R.; Rehman, R. U. Synergistic effect of plant extract coupled silver nanoparticles in various therapeutic applications-present insights and bottlenecks. *Chemosphere* **2022**, *288*, 132527.
(39) (a) Asfaw, N.; Demissew, S. Essential oil composition of four Artemisia Species from Ethiopia. *Bull. Chem. Soc. Ethiop.* **2015**, *29* (1), 123−128. (b) Tesfahuneygn, G.; Gebreegziabher, G. Medicinal plants used in traditional medicine by Ethiopians: a review article. *J. Respir. Med. Lung Dis.* **2019**, *4* (1), 1−3.

https://doi.org/10.1021/acsomega.3c01814
ACS Omega 2023, 8, 41039−41053

(40) (a) d'Avigdor, E.; Wohlmuth, H.; Asfaw, Z.; Awas, T. The current status of knowledge of herbal medicine and medicinal plants in Fiche, Ethiopia. *J. Ethnobiol. Ethnomed.* **2014**, *10* (1), 38. (b) Ayalew, H.; Tewelde, E.; Abebe, B.; Alebachew, Y.; Tadesse, S. Endemic medicinal plants of Ethiopia: Ethnomedicinal uses, biological activities and chemical constituents. *J. Ethnopharmacol.* **2022**, *293*, 115307. (c) Adugna, M.; Feyera, T.; Taddese, W.; Admasu, P. In vivo antimalarial activity of crude extract of aerial part of Artemisia abyssinica against Plasmodium berghei in mice. *Global J. Pharmacol.* **2014**, *8* (3), 460−468.

(41) Letha, N.; Ganesan, K.; Nair, S. K. P.; Gani, S. Studies on phytochemical screening and in vitro antioxidant activity of Ethiopian indigenous medicinal Plants, Artemisia abyssinica Sch. Bip. ex A. Rich. *World J. Pharmaceut. Res.* **2016**, *5*, 1048−1058.

(42) Elemike, E. E.; Onwudiwe, D. C.; Nundkumar, N.; Singh, M.; Iyekowa, O. Green synthesis of Ag, Au and Ag-Au bimetallic nanoparticles using Stigmaphyllon ovatum leaf extract and their in vitro anticancer potential. *Mater. Lett.* **2019**, *243*, 148−152.

(43) Benzie, I. F.; Strain, J. J. The ferric reducing ability of plasma (FRAP) as a measure of "antioxidant power": the FRAP assay. *Anal. Biochem.* **1996**, *239* (1), 70−76.

(44) Chau, T. P.; Veeraragavan, G. R.; Narayanan, M.; Chinnathambi, A.; Alharbi, S. A.; Subramani, B.; Brindhadevi, K.; Pimpimon, T.; Pikulkaew, S. Green synthesis of Zirconium nanoparticles using Punica granatum (pomegranate) peel extract and their antimicrobial and antioxidant potency. *Environ. Res.* **2022**, *209*, 112771.

(45) Sirivibulkovit, K.; Nouanthavong, S.; Sameenoi, Y. Paper-based DPPH Assay for Antioxidant Activity Analysis. *Anal. Sci.* **2018**, *34* (7), 795−800.

(46) Dekkers, J. F.; van Vliet, E. J.; Sachs, N.; Rosenbluth, J. M.; Kopper, O.; Rebel, H. G.; Wehrens, E. J.; Piani, C.; Visvader, J. E.; Verissimo, C. S.; et al. Long-term culture, genetic manipulation and xenotransplantation of human normal and breast cancer organoids. *Nat. Protoc.* **2021**, *16* (4), 1936−1965.

(47) (a) Rai, Y.; Pathak, R.; Kumari, N.; Sah, D. K.; Pandey, S.; Kalra, N.; Soni, R.; Dwarakanath, B.; Bhatt, A. N. Mitochondrial biogenesis and metabolic hyperactivation limits the application of MTT assay in the estimation of radiation induced growth inhibition. *Sci. Rep.* **2018**, *8* (1), 1531. (b) Nga, N.; Ngoc, T.; Trinh, N.; Thuoc, T.; Thao, D. Optimization and application of MTT assay in determining density of suspension cells. *Anal. Biochem.* **2020**, *610*, 113937.

(48) Morris, G. M.; Huey, R.; Lindstrom, W.; Sanner, M. F.; Belew, R. K.; Goodsell, D. S.; Olson, A. J. AutoDock4 and AutoDockTools4: Automated docking with selective receptor flexibility. *J. Comput. Chem.* **2009**, *30* (16), 2785−2791.

(49) Khalil, A. T.; Ayaz, M.; Ovais, M.; Wadood, A.; Ali, M.; Shinwari, Z. K.; Maaza, M. In vitro cholinesterase enzymes inhibitory potential and in silico molecular docking studies of biogenic metal oxides nanoparticles. *Inorg. Nano-Met. Chem.* **2018**, *48* (9), 441−448.

(50) Murthy, H.; Desalegn, T.; Kassa, M.; Abebe, B.; Assefa, T. Synthesis of green copper nanoparticles using medicinal plant hagenia abyssinica (Brace) JF. Gmel. leaf extract: Antimicrobial properties. *J. Nanomater.* **2020**, *2020*, 1−12.

(51) Thamer, N.; Muftin, N.; Al-Rubae, S. Optimization properties and characterization of green synthesis of copper oxide nanoparticles using aqueous extract of Cordia myxa L. leaves. *Asian J. Chem.* **2018**, *30* (7), 1559−1563.

(52) Desalegn, T.; Murthy, H.; Ravikumar, C.; Nagaswarupa, H. Green Synthesis of CuO Nanostructures using Syzygium guineense (Willd.) DC Plant Leaf Extract and Their Applications. *J. Nanostruct.* **2021**, *11* (1), 81−94.

(53) Al Mamari, H. H. *Phenolic compounds: Classification, chemistry, and updated techniques of analysis and synthesis*; IntechOpen, 2021; Vol. *10*.

(54) Elemike, E. E.; Onwudiwe, D. C.; Singh, M. Eco-friendly synthesis of copper oxide, zinc oxide and copper oxide-zinc oxide nanocomposites, and their anticancer applications. *J. Inorg. Organomet. Polym. Mater.* **2020**, *30*, 400−409.

(55) Mlalila, N. G.; Swai, H. S.; Hilonga, A.; Kadam, D. M. Antimicrobial dependence of silver nanoparticles on surface plasmon resonance bands against Escherichia coli. *Nanotechnol. Sci. Appl.* **2016**, *10*, 1−9.

(56) Majhi, J. K.; Kuiri, P. K. Large spectral shift of plasmon resonances in Au-Cu alloy nanoparticles through anisotropy and interaction. *Bull. Mater. Sci.* **2021**, *44* (1), 18.

(57) Vinu, D.; Govindaraju, K.; Vasantharaja, R.; Amreen Nisa, S.; Kannan, M.; Vijai Anand, K. Biogenic zinc oxide, copper oxide and selenium nanoparticles: preparation, characterization and their antibacterial activity against Vibrio parahaemolyticus. *J. Nanostruct. Chem.* **2021**, *11* (2), 271−286.

(58) Ajitha, B.; Kumar Reddy, Y. A.; Reddy, P. S.; Jeon, H.-J.; Ahn, C. W. Role of capping agents in controlling silver nanoparticles size, antibacterial activity and potential application as optical hydrogen peroxide sensor. *RSC Adv.* **2016**, *6* (42), 36171−36179.

(59) Annathurai, S.; Chidambaram, S.; Baskaran, B.; Prasanna Venkatesan, G. Green synthesis and electrical properties of p-CuO/n-ZnO heterojunction diodes. *J. Inorg. Organomet. Polym. Mater.* **2019**, *29* (2), 535−540.

(60) Narendhran, S.; Sivaraj, R. Biogenic ZnO nanoparticles synthesized using L. aculeata leaf extract and their antifungal activity against plant fungal pathogens. *Bull. Mater. Sci.* **2016**, *39*, 1−5.

(61) (a) Karthik, K.; Raghu, A.; Reddy, K. R.; Ravishankar, R.; Sangeeta, M.; Shetti, N. P.; Reddy, C. V. Green synthesis of Cu-doped ZnO nanoparticles and its application for the photocatalytic degradation of hazardous organic pollutants. *Chemosphere* **2022**, *287*, 132081. (b) Ekinci, A.; Kutluay, S.; Şahin, O.··.; Baytar, O. Green synthesis of copper oxide and manganese oxide nanoparticles from watermelon seed shell extract for enhanced photocatalytic reduction of methylene blue. *Int. J. Phytoremediation* **2023**, *25* (6), 789−798.

(62) (a) Munguti, L.; Dejene, F. Effects of Zn: Ti molar ratios on the morphological, optical and photocatalytic properties of ZnO-TiO2 nanocomposites for application in dye removal. *Mater. Sci. Semicond. Process.* **2021**, *128*, 105786. (b) Mazabuel-Collazos, A.; Gómez, C. D.; Rodríguez-Páez, J. ZnO-TiO2 nanocomposites synthesized by wet-chemical route: study of their structural and optical properties. *Mater. Chem. Phys.* **2019**, *222*, 230−245.

(63) Rajagopal, G.; Nivetha, A.; Sundar, M.; Panneerselvam, T.; Murugesan, S.; Parasuraman, P.; Kumar, S.; Ilango, S.; Kunjiappan, S. Mixed phytochemicals mediated synthesis of copper nanoparticles for anticancer and larvicidal applications. *Heliyon* **2021**, *7* (6), No. e07360.

(64) Lv, Q.; Zhang, B.; Xing, X.; Zhao, Y.; Cai, R.; Wang, W.; Gu, Q. Biosynthesis of copper nanoparticles using Shewanella loihica PV-4 with antibacterial activity: Novel approach and mechanisms investigation. *J. Hazard Mater.* **2018**, *347*, 141−149.

(65) Sarwar, N.; Humayoun, U. B.; Kumar, M.; Zaidi, S. F. A.; Yoo, J. H.; Ali, N.; Jeong, D. I.; Lee, J. H.; Yoon, D. H. Citric acid mediated green synthesis of copper nanoparticles using cinnamon bark extract and its multifaceted applications. *J. Clean. Prod.* **2021**, *292*, 125974.

(66) Umaralikhan, L.; Jamal Mohamed Jaffar, M. Green synthesis of MgO nanoparticles and it antibacterial activity. *Iran. J. Sci. Technol. Trans. A Sci.* **2018**, *42* (2), 477−485.

(67) Jayachandran, A.; Tr, A.; Nair, A. S. Green synthesis and characterization of zinc oxide nanoparticles using Cayratia pedata leaf extract. *Biochem. Biophys. Rep.* **2021**, *26*, 100995.

(68) Darroudi, M.; Sabouri, Z.; Kazemi Oskuee, R.; Khorsand Zak, A.; Kargar, H.; Hamid, M. H. N. A. Sol-gel synthesis, characterization, and neurotoxicity effect of zinc oxide nanoparticles using gum tragacanth. *Ceram. Int.* **2013**, *39* (8), 9195−9199.

(69) Tabrizi Hafez Moghaddas, S. M.; Elahi, B.; Javanbakht, V. Biosynthesis of pure zinc oxide nanoparticles using Quince seed mucilage for photocatalytic dye degradation. *J. Alloys Compd.* **2020**, *821*, 153519.

(70) Lozhkomoev, A.; Bakina, O.; Pervikov, A.; Kazantsev, S.; Glazkova, E. Synthesis of CuO-ZnO composite nanoparticles by

https://doi.org/10.1021/acsomega.3c01814
ACS Omega 2023, 8, 41039−41053

electrical explosion of wires and their antibacterial activities. *J. Mater. Sci.: Mater. Electron.* **2019**, *30*, 13209−13216.
(71) Soleimani-Amiri, S.; Hossaini, Z.; Azizi, Z. Synthesis and Investigation of Biological Activity of New Oxazinoazepines: Application of Fe3O4/CuO/ZnO@ MWCNT Magnetic Nanocomposite in Reduction of 4-Nitrophenol in Water. *Polycyclic Aromat. Compd.* **2023**, *43* (4), 2938−2959.
(72) Djamila, B.; Eddine, L. S.; Abderrhmane, B.; Nassiba, A.; Barhoum, A. In vitro antioxidant activities of copper mixed oxide (CuO/Cu2O) nanoparticles produced from the leaves of Phoenix dactylifera L. *Biomass Conversion and Biorefinery*; Springer, 2022.
(73) Lal, S.; Verma, R.; Chauhan, A.; Dhatwalia, J.; Guleria, I.; Ghotekar, S.; Thakur, S.; Mansi, K.; Kumar, R.; Kumari, A.; et al. Antioxidant, antimicrobial, and photocatalytic activity of green synthesized ZnO-NPs from Myrica esculenta fruits extract. *Inorg. Chem. Commun.* **2022**, *141*, 109518.
(74) (a) Suresh, P.; Doss, A.; Praveen Pole, R.; Devika, M. Green synthesis, characterization and antioxidant activity of bimetallic (Ag-ZnO) nanoparticles using Capparis zeylanica leaf extract. *Biomass Convers. Biorefin.* **2023**, 1−9. (b) Riaz, T.; Assey, N.; Javed, M.; Shahzadi, T.; Zaib, M.; Shahid, S.; Iqbal, S.; Elkaeed, E. B.; Alzhrani, R. M.; Alsaab, H. O.; et al. Biogenic plant mediated synthesis of monometallic zinc and bimetallic Copper/Zinc nanoparticles and their dye adsorption and antioxidant studies. *Inorg. Chem. Commun.* **2022**, *140*, 109449.
(75) Khonkarn, R.; Okonogi, S.; Ampasavate, C.; Anuchapreeda, S. Investigation of fruit peel extracts as sources for compounds with antioxidant and antiproliferative activities against human cell lines. *Food Chem. Toxicol.* **2010**, *48* (8−9), 2122−2129.
(76) Ioset, J.-R.; Brun, R.; Wenzler, T.; Kaiser, M.; Yardley, V. *Drug screening for kinetoplastids diseases: A training manual for screening in neglected diseases*, 2009.
(77) Zughaibi, T. A.; Mirza, A. A.; Suhail, M.; Jabir, N. R.; Zaidi, S. K.; Wasi, S.; Zawawi, A.; Tabrez, S. Evaluation of anticancer potential of biogenic copper oxide nanoparticles (CuO NPs) against breast cancer. *J. Nanomater.* **2022**, *2022*, 1−7.
(78) Dey, A.; Manna, S.; Chattopadhyay, S.; Mondal, D.; Chattopadhyay, D.; Raj, A.; Das, S.; Bag, B. G.; Roy, S. Azadirachta indica leaves mediated green synthesized copper oxide nanoparticles induce apoptosis through activation of TNF-α and caspases signaling pathway against cancer cells. *J. Saudi Chem. Soc.* **2019**, *23* (2), 222−238.
(79) Raj Preeth, D.; Shairam, M.; Suganya, N.; Hootan, R.; Kartik, R.; Pierre, K.; Suvro, C.; Rajalakshmi, S. Green synthesis of copper oxide nanoparticles using sinapic acid: an underpinning step towards antiangiogenic therapy for breast cancer. *JBIC, J. Biol. Inorg. Chem.* **2019**, *24* (5), 633−645.
(80) Bhatt, S.; Stender, J.; Joshi, S.; Wu, G.; Katzenellenbogen, B. OCT-4: a novel estrogen receptor-α collaborator that promotes tamoxifen resistance in breast cancer cells. *Oncogene* **2016**, *35* (44), 5722−5734.

https://doi.org/10.1021/acsomega.3c01814
ACS Omega 2023, 8, 41039−41053